aemic insult. In this regard, several experimental and clinical investigators have compared the [^{123}I]IMZ distribution with the cerebral blood flow, oxygen metabolism and/or glucose metabolism, and shown the potential of [^{123}I]IMZ for evaluation of neuronal viability after an ischaemic stroke [3, 6, 7, 8, 9, 10, 11, 12]. A few authors [6, 10, 11] have also correlated [^{123}I]IMZ distribution with histological findings obtained using the haematoxylin-eosin stain.

To the best of our knowledge, however, the brain distribution of [^{123}I]IMZ has not been correlated with the molecular response after an ischaemic insult in detail. The pathophysiological significance of findings that are actually imaged by [^{123}I]IMZ also remains to be elucidated. Accordingly, we compared the brain distribution of [^{123}I]IMZ with (1) cerebral blood flow, (2) the expression of cyclooxygenase-2 (COX-2), (3) fragmentation of DNA and (4) cellular integrity, in order to characterise [^{123}I]IMZ as a marker of neuronal viability. COX-2, a prostanoid synthesising enzyme, is expressed early after an ischaemic insult and contributes to the progression of ischaemic damage [13, 14, 15, 16, 17]. Thus, we examined COX-2 expression to evaluate the neuronal response early after an ischaemic insult. In situ DNA polymerase-I-dependent dUTP incorporation into damaged DNA was used as an indicator of DNA fragmentation. Techniques for visual detection and localisation of DNA injury/repair in situ include: TdT-dependent dUTP labelling of free 3'-OH ends of double-stranded DNA (TUNEL); Klenow fragment of DNA polymerase-I-dependent labelling of staggered 3'-OH ends and gaps; and DNA polymerase-I incorporation in nicks, gaps and staggered 3'-OH ends [18]. Of these, only DNA polymerase-I has 5'–>3' exonucleolytic activity, which allows nick translation and visualisation of randomly occurring single-strand scission of double-stranded DNA. MAP-2, a cellular structural protein existing on the surface of neurodendrites, is also immunostained as a marker of cellular integrity.

Materials and methods

Animal preparation. The experimental protocol was fully approved by the Laboratory Animal Care and Use Committee of Hokkaido University. Male Sprague-Dawley rats weighing 300–350 g were used. The rats had free access to water and laboratory chow. The animals were initially anaesthetised with 400 mg/kg body weight IP chloral hydrate. The body temperatures were monitored with rectal probes and maintained at 37°C with heating pads during the operation. The rats were subjected to permanent unilateral major artery occlusion. The right middle cerebral artery (MCA) of each rat was occluded intraluminally according to a method described in detail previously [19, 20, 21]. The rats were allowed to recover from anaesthesia and any induced neurological deficits were confirmed. The animals not showing any neurological deficits were excluded from this experiment.

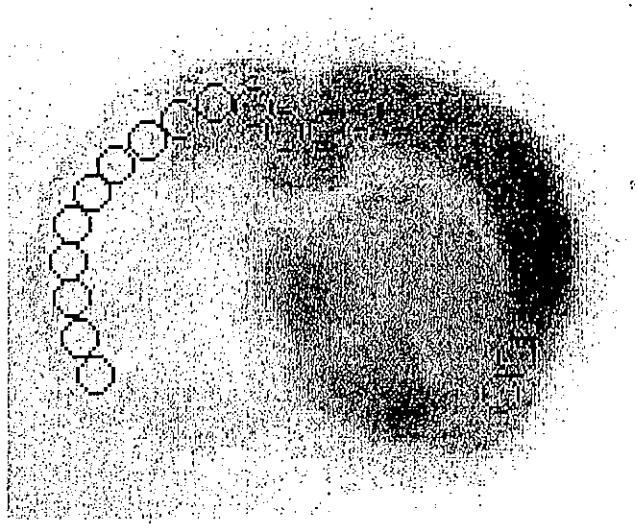

Fig. 1. An example of regions of interest (ROIs) on a coronal image. Twelve circular ROIs (2 mm in diameter) were determined on each hemisphere of the cortex symmetrically

Autoradiographic studies. The brain distributions of [^{123}I]IMZ and [^{125}I]IMP were determined using a dual-tracer autoradiographic technique. [^{123}I]IMZ (111 MBq/kg body weight) was first injected via the femoral vein 60 min before decapitation, to determine specific [^{123}I]IMZ distribution according to the methods reported by Toyama et al. [10, 11]. Then, 55 min later, [^{125}I]IMP (2.22 MBq/kg body weight) was injected via the contralateral femoral vein, to assess blood flow distribution [10, 11]. The rats were decapitated under chloral hydrate anaesthesia 5 min after the injection of [^{125}I]IMP, which was 2, 3, 4, 6, 8, 12 and 24 h after the ischaemic insult (n = four to six in each group). Their brains were removed quickly and carefully, and immersed in ice-cold saline. The brains were then sectioned at 6 mm caudal from the frontal pole using a brain matrix (RBM-4000C, ASI Instruments, Warren, MI) to obtain coronal sections. The brain samples were embedded in a medium (Tissue-Tek, Sakura Finetechnical Co., Ltd., Tokyo, Japan), frozen in isopentane-dry ice, and cut into 20-μm sections with a cryostat (Bright Instrument Co., Ltd., Cambridgeshire, England). The first autoradiographic exposure was performed for 3 h to detect the distribution of [^{123}I]IMZ. The second exposure was initiated 7 days later and carried out for 7 days to visualise the distribution of [^{125}I]IMP.

Histological studies. Immunoreactivity to COX-2 and microtubule-associated protein-2 (MAP-2) were detected in frozen sections (10 μm thick) adjacent to those used for the autoradiographic studies, using a standard immunostaining procedure [23]. Briefly, after fixation in a cold 1:1 acetone-to-methanol mixture, the sections were incubated with a polyclonal anti-COX-2 antibody (Cayman Chemical; dilution 1:2,000) or a purified mouse monoclonal anti-MAP-2 antibody (BD Pharmingen, San Diego; dilution 1:400). The bound antibody was visualised by staining with avidin/biotin conjugate immunoperoxidase (Vector Laboratories, Inc., CA, USA) and 3,3'-diaminobenzidine tetrahydrochloride (DAB; Vectastain Elite Kit, Vector Laboratories, CA).

DNA fragmentation was also detected on the adjacent sections by incorporation of digoxigenin-dUTP using DNA polymerase-I according to the method previously described [18, 23]. To confirm the nuclear localisation of the label, some sections were counterstained with haematoxylin.

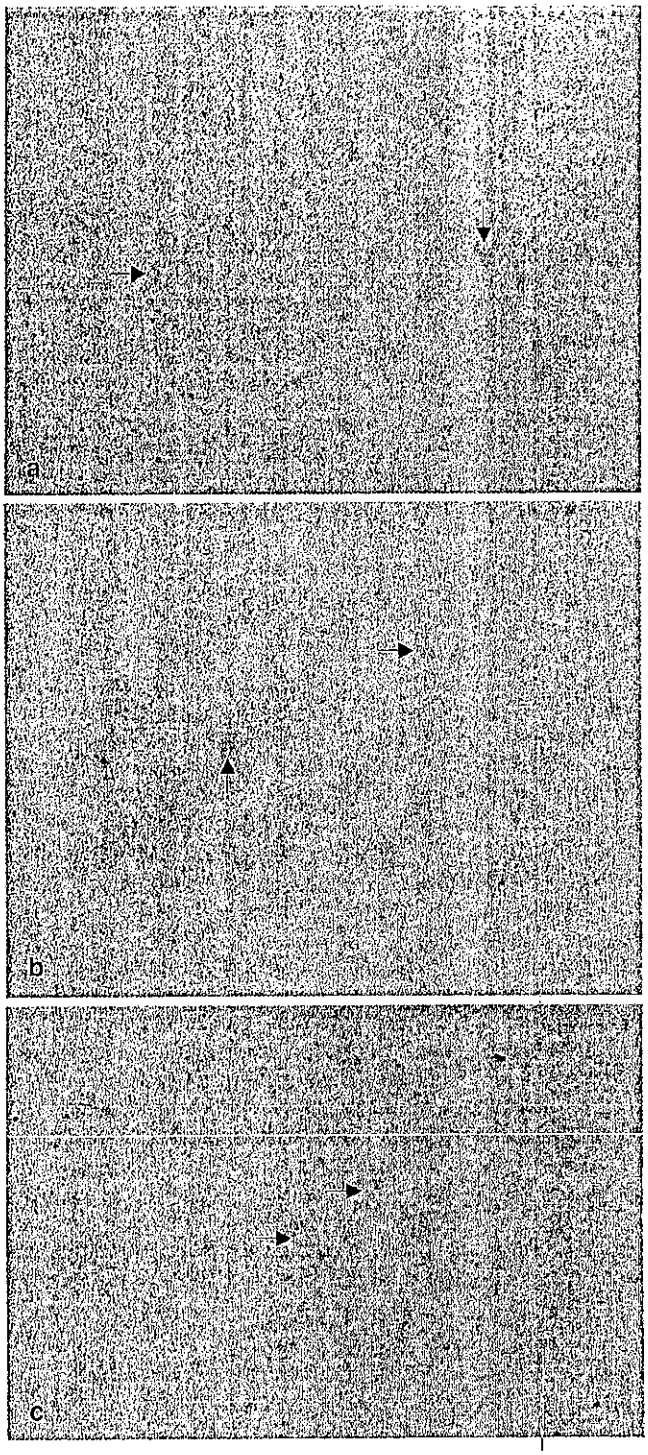

Data analysis. The autoradiograms were analysed using a computerised imaging analysis system (Bio-imaging Analyser BAS-5000, Fuji Photo Film, Tokyo, Japan). To quantitatively evaluate the distributions of [^{123}I]IMZ and [^{125}I]IMP, 12 circular regions of interest (ROIs, 2 mm in diameter) were determined on each hemisphere of the cerebral cortex in the autoradiograms symmetrically from the longitudinal fissure to the temporal lobe (Fig. 1). Lesion to normal ratios (LNRs) were defined as the ratios of values for an ROI in the lesioned hemisphere to those for the contralateral homologous ROI.

Based on the LNRs for [^{123}I]IMZ and [^{125}I]IMP, ROIs determined on the lesioned hemisphere were classified into three groups as shown in Table 1: group 1, LNRs for both [^{125}I]IMP and [^{123}I]IMZ were equal to or larger than 0.8; group 2, the LNRs for [^{125}I]IMP were less than 0.8 and those for [^{123}I]IMZ were equal to or larger than 0.8; group 3, LNRs for both [^{125}I]IMP and [^{123}I]IMZ were less than 0.8. A threshold LNR of 0.8 was chosen, considering the lesion detectability by the autoradiographic methods [11].

The ROIs determined on the lesioned hemisphere were also classified into four groups based on histological findings as follows (Fig. 2): group A, impaired MAP-2 immunostaining; group B, preserved MAP-2 immunostaining and positive for dUTP incorporation; group C, preserved MAP-2 immunostaining, negative for dUTP incorporation and positive for COX-2; group D, no histological evidence of an ischaemic injury.

All values are expressed as means or means ± standard deviation. A Z test was used to assess the significance of difference in the percentage of ROIs with impaired [^{125}I]IMP or [^{123}I]IMZ accumulation. One-way ANOVA and post-hoc tests (Fisher's method) were used to assess the significance of difference in the LNRs among the four groups classified on the basis of histological findings. A two-tail value of $P<0.05$ was considered to indicate statistical significance.

Results

Figure 3 shows representative autoradiograms for [^{125}I]IMP and [^{123}I]IMZ. The accumulation of [^{125}I]IMP decreased in a wide region in the MCA territory 2 h after occlusion, which extended with time. The region with

Fig. 2a–c. Representative images of **a** COX-2 immunostaining (×200), **b** dUTP incorporation (×200) and **c** MAP-2 immunostaining (×200). **a** Expression of COX-2 protein was occasionally observed (*arrows*). **b** The ring-like appearance (*arrows*) of dUTP incorporation shows the neuron on the way to apoptotic cell death. **c** Positive MAP-2 immunostaining (*arrows*) shows cellular integrity

Table 1. Histological findings in the three ROI groups classified on the basis of LNRs

Group	LNR_{IMP}	LNR_{IMZ}	Number (%) of ROIs		
			COX-2 (+)	dUTP (+)	MAP-2 (–)
Group 1 (n=14)	≥0.8	≥0.8	0 (0%)	0 (0%)	0 (0%)
Group 2 (n=24)	<0.8	≥0.8	4 (16.7%)	0 (0%)	0 (0%)
Group 3 (n=238)	<0.8	<0.8	79 (33.2%)	59 (24.8%)	176 (73.9%)

LNR_{IMP}, LNR for [^{125}I]IMP; LNR_{IMZ}, LNR for [^{123}I]IMZ; COX-2 (+), positive immunostaining for COX-2; dUTP (+), positive dUTP incorporation; MAP-2 (–), negative immunostaining for MAP-2

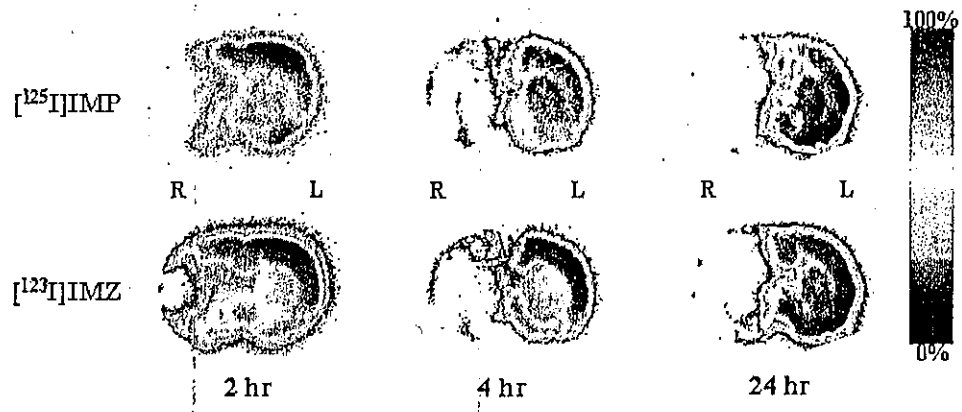

Fig. 3. Representative autoradiograms for [125I]IMP and [123I]IMZ

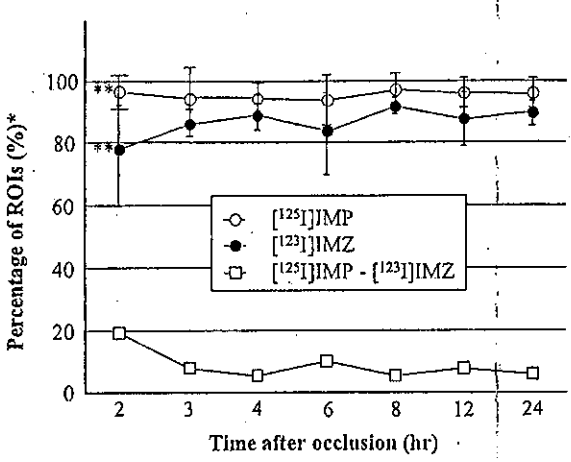

Fig. 4. Time course of the percentage of ROIs with impaired [125I]IMP or [123I]IMZ accumulation. *(Number of ROIs with LNRs less than 0.8)/(Number of total ROIs at each time point) ×100. ROIs with impaired [125I]IMP and [123I]IMZ accumulation were defined as those with LNRs less than 0.8. Significant uncoupling of accumulation between the two tracers was observed 2 h after occlusion (**P<0.01)

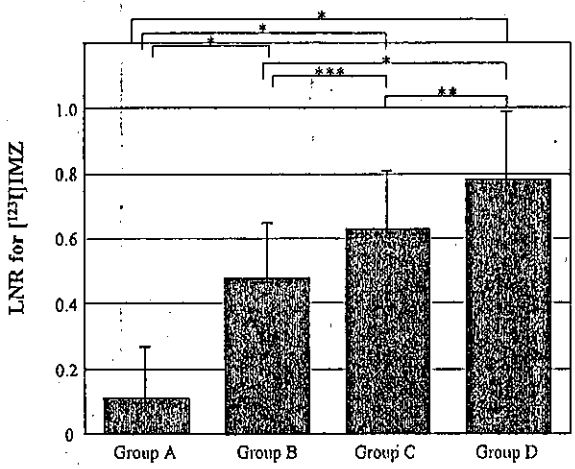

Fig. 5. The LNRs for [123I]IMZ in the four ROI groups classified on the basis of histological findings. Group A, impaired MAP-2 immunostaining; group B, preserved MAP-2 immunostaining and positive dUTP incorporation; group C, preserved MAP-2 immunostaining, negative dUTP incorporation and positive COX-2 immunostaining; group D, no histological evidence of ischaemic injury. Significant differences in LNRs between two groups: *P<0.0001, **P<0.001, ***P<0.01

decreased [123I]IMZ accumulation was smaller than that with decreased [125I]IMP accumulation (P<0.01). Uncoupling between [125I]IMP and [123I]IMZ accumulation was observed in regions surrounding the ischaemic core 2 h after occlusion, but such uncoupling reduced with time. The percentage of ROIs with impaired [123I]IMZ accumulation was significantly lower than that with decreased [125I]IMP accumulation at 2 h after occlusion (P<0.01), but not at other time points (Fig. 4).

Positivity for COX-2 was observed in 16.7% of the ROIs in the ischaemic lesions with preserved [123I]IMZ distribution (group 2) and 33.2% of the ROIs in the ischaemic lesions with decreased [123I]IMZ distribution (group 3), whereas no positivity for COX-2 was seen in non-ischaemic lesions (group 1) (Table 1). Neither positivity for dUTP incorporation nor decreased immunostaining of MAP-2 was observed in the ROIs in the lesions with preserved [123I]IMZ distribution (groups 1 and 2). Positivity for dUTP incorporation and impaired MAP-2 immunostaining were observed in 24.8% and 73.9% of the ROIs, respectively, in the lesions with decreased [123I]IMZ distribution (group 3) (Table 1).

When the ROIs were divided into four groups based on the histological findings (Fig. 5), the LNRs for [123I]IMZ in the lesions with preserved MAP-2 immunostaining (groups B, C and D) were significantly higher than those in the lesions with impaired MAP-2 immunostaining (group A; P<0.0001). The LNRs for [123I]IMZ in the lesions with preserved MAP-2 immunostaining and positive for dUTP incorporation (group B) were significantly lower than those in the lesions with preserved MAP-2 immunostaining and negative for dUTP incorporation (groups C; P<0.01, group D; P<0.0001). The LNRs for [123I]IMZ in the lesions with preserved MAP-2 immunostaining, negative for dUTP incorporation and positive for COX-2 (group C) were significantly lower

than those in the lesions with no histological evidence of an ischaemic injury (group D; $P<0.001$).

Discussion

In order to characterise [^{123}I]IMZ as a marker of neuronal viability, we compared the brain distribution of [^{123}I]IMZ with the expression of COX-2, DNA fragmentation and cellular integrity. Neither DNA fragmentation nor MAP-2 denaturation was detected in the ischaemic regions with preserved [^{123}I]IMZ accumulation. These results clearly demonstrate that neuronal DNA is still intact and cellular integrity is maintained in the ischaemic regions with preserved [^{123}I]IMZ accumulation. COX-2 expression was often observed in these regions. In addition, semiquantitative analysis based on the histological findings showed that [^{123}I]IMZ accumulation was significantly impaired in regions where DNA fragmentations were observed. Thus, [^{123}I]IMZ distribution can be an indicator that predicts the extent of neuronal damage after an ischaemic stroke.

In the present study, we compared the brain distribution of [^{123}I]IMZ with (1) CBF, (2) the expression of COX-2, a prostanoid synthesising enzyme that contributes to the progression of ischaemic damage [13, 14, 15, 16, 17], (3) fragmentation of DNA and (4) cellular integrity. The regions with preserved [^{123}I]IMZ accumulation and decreased [^{125}I]IMP accumulation, namely, uncoupling between CBF and BZR function, were observed 2 h after occlusion in regions surrounding the ischaemic core, which became smaller with time. Such uncoupling has been observed in the acute phase by several authors [9, 24, 25]. The BZR function in these regions can be regarded as intact in spite of hypoperfusion. Clinically, it was reported that the hypoperfused regions with preserved [^{123}I]IMZ accumulation do not develop infarction as determined in a follow-up evaluation with magnetic resonance imaging [3]. The uncoupling between [^{125}I]IMP and [^{123}I]IMZ accumulation may help determine the ischaemic penumbra.

Some authors [6, 10, 11] have compared [^{123}I]IMZ distribution with histological findings obtained using the haematoxylin-eosin stain. They suggested the potential of [^{123}I]IMZ for evaluating the extent of neuronal damage. The brain distribution of [^{123}I]IMZ, however, has not been correlated with the cellular response at the molecular level. The present results on the relationship between [^{123}I]IMZ accumulation and dUTP incorporation clearly demonstrate that neuronal DNA is still intact in the ischaemic regions where [^{123}I]IMZ accumulation is preserved. In addition, our results indicate the potential of [^{123}I]IMZ to significantly detect the region with DNA scission as a reduction in LNRs. It was reported that COX-2 is expressed early after an ischaemic insult and leads ischaemic neurons to apoptotic cell death [17, 26]. In the present study, COX-2 expression was often observed in the ischaemic regions with preserved [^{123}I]IMZ accumulation. COX-2 expression may precede impairment of [^{123}I]IMZ accumulation. On the other hand, the COX-2 protein was also observed in the regions where [^{123}I]IMZ accumulation decreased. The LNRs for [^{123}I]IMZ accumulation in group C (0.626±0.186) were significantly lower than those in group D (0.783±0.213). The role of the COX-2 protein may begin before the impairment of BZR function and it may continue even after this impairment, although further investigations are required to clarify this point. These results indicate that impairment of [^{123}I]IMZ accumulation may begin as early as the COX-2 expression after an acute stroke.

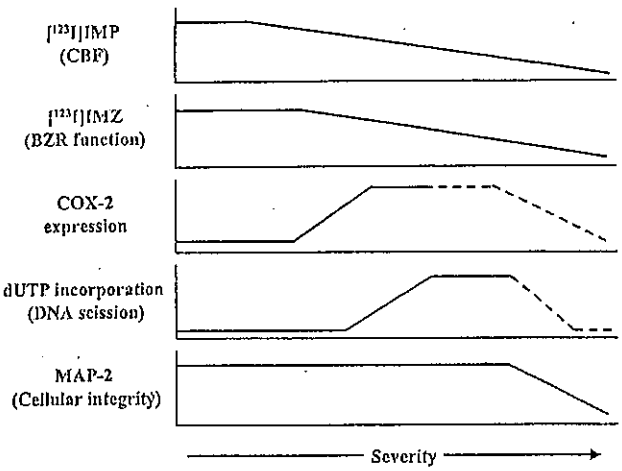

Fig. 6. Schematic representation of possible relationship between tracer accumulation and pathophysiological changes

From our results, a possible relationship between tracer accumulation and pathophysiological changes can be summarised as shown in Fig. 6. Namely, [^{125}I]IMP accumulation decreases concurrently with CBF after an ischaemic insult. COX-2 expression is often observed early after the ischaemic insult. [^{123}I]IMZ accumulation, namely, the BZR function, was impaired at a similar stage to COX-2 expression. DNA scission and impairment of cellular integrity follow the reduction in [^{123}I]IMZ accumulation.

Methodological considerations

In a clinical setting, an interval of several hours is required to sufficiently characterise BZR distribution after the [^{123}I]IMZ injection. In this study, however, rats were sacrificed 60 min after [^{123}I]IMZ administration, according to the method reported by Toyama et al. [10]. Their kinetic study indicated that specific binding of [^{123}I]IMZ can be evaluated 60 min after [^{123}I]IMZ injection in a rat model of cerebral ischaemia. Specific distribution of [^{123}I]IMZ can be achieved in a shorter period of 60 min in rats.

The relationship between tracer distribution and histological findings was evaluated simultaneously, using all samples obtained from rats sacrificed at variable time intervals after the ischaemic insult, in order to characterise [^{123}I]IMZ distribution in regions with ischaemic injury of various extent. Regional analysis in rats subjected to the same period of MCA occlusion may provide more precise information on the relationship. The relatively narrow penumbra in rats, however, may restrict such evaluation and require a higher number of rats. Thus, in the present study, the relationship was evaluated simultaneously in rats sacrificed at variable time intervals.

The average LNR for [^{123}I]IMZ in histologically normal regions was not higher than 0.8. Although, in this study, we chose 0.8 as the threshold value of the LNRs for [^{123}I]IMZ, further examinations may be needed to determine a more suitable threshold value of LNR for [^{123}I]IMZ.

In the present study, we used a dual-tracer autoradiographic technique to evaluate the blood flow and [^{123}I]IMZ binding in the same individuals. Consequently, we could not perform quantitative assessment of the blood flow and [^{123}I]IMZ binding, as it is methodologically difficult to quantitatively assess flow and IMZ binding using the dual-tracer autoradiographic technique. Further studies, especially on quantitative measurement of flow and [^{123}I]IMZ binding, are required to confirm the present results and to obtain relevant information on the flow and [^{123}I]IMZ binding in relation to the histopathological findings.

Clinical implications

The routine use of nuclear medicine for the clinical assessment of neuronal viability has been limited exclusively to the determination of CBF, oxygen and/or glucose consumption, and CBF reactivity to acetazolamide. Oxygen and glucose metabolism and CBF reactivity to acetazolamide, however, do not provide direct information on neuronal viability. Rather, these techniques yield information not only on neurons but also on astrocytes and Schwann cells. On the other hand, [^{123}I]IMZ, a central-type BZR ligand, can be a specific marker of neuronal viability. Heiss et al. suggested that imaging of BZR receptors could distinguish between irreversibly damaged and viable penumbra tissues immediately after an acute stroke using carbon-11 flumazenil and positron emission tomography [27, 28]. The present study in the rat model demonstrated that [^{123}I]IMZ can also be a marker for neuronal viability. In addition, [^{123}I]IMZ does not require in-house cyclotrons and positron emission tomography, and can be commercially supplied. The availability of this procedure is expected to favour the clinical application of [^{123}I]IMZ.

Conclusion

The present study demonstrated for the first time that impairment of [^{123}I]IMZ accumulation precedes DNA fragmentation and denaturation of cellular integrity. Our results provide the molecular basis of [^{123}I]IMZ distribution. [^{123}I]IMZ accumulation can be a clue to predicting the severity of ischaemic neuronal injury.

Acknowledgement. The authors are grateful to Professors S. Nishi, K. Miyasaka and T. Ohnishi of the Central Institute of Isotope Science, Hokkaido University, for supporting this work. We also express gratitude to Drs. T. Abumiya and K. Hikosaka for helpful discussions.

This work was supported in part by a Grant-in-Aid for Scientific Research from the Japan Society for the Promotion of Science, and Grants from Japan Heart Foundation Research, the Takeda Medical Research Foundation in Japan and the Mitubishi Pharma Research Foundation in Japan.

References

1. Garcia JH, Lassen NA, Weiller C, Sperling B, Nakagawara J. Ischemic stroke and incomplete infarction. *Stroke* 1996; 27:761–765.
2. Garcia JH, Liu KF, Ye ZR, Gutierrez JA. Incomplete infarct and delayed neuronal death after transient middle cerebral artery occlusion in rats. *Stroke* 1997; 28:2303–2310.
3. Nakagawara J, Sperling B, Lassen NA. Incomplete brain infarction of reperfused cortex may be quantitated with iomazenil. *Stroke* 1997; 28:124–132.
4. Heiss WD, Graf R, Fujita T, Ohta K, Bauer B, Lötten J, Wienhard K. Early detection of irreversibly damaged ischemic tissue by flumazenil positron emission tomography in cats. *Stroke* 1997; 28:2045–2052.
5. Heiss WD, Kracht LW, Thiel A, Grond M, Pawlik G. Penumbral probability thresholds of cortical flumazenil binding and blood flow prediction tissue outcome in patients with cerebral ischaemia. *Brain* 2001; 124:20–29.
6. Odano I, Miyashita K, Minoshima S, Nakajima T, Fujita M, Takahashi N, Ikuta F. A potential use of a ^{123}I-labeled benzodiazepine antagonist as a predictor of neuronal call viability: comparisons with ^{14}C-labeled 2-deoxyglucose autoradiography and histological examination. *Nucl Med Commun* 1996; 16:443–446.
7. Matsuda H, Tsuji S, Kuji I, Shiba K, Hisada K, Mori H. Dual-tracer autoradiography using ^{125}I-iomazenil and ^{99m}Tc-HMPAO in experimental brain ischemia. *Nucl Med Commun* 1995; 16:581–590.
8. Hatazawa J, Shimosegawa E, Satoh T, Kanno I, Uemura K. Central benzodiazepine receptor distribution after subcortical hemorrhage evaluated by means of [^{123}I]IMZ and SPECT. *Stroke* 1995; 26:2267–2271.
9. Dong Y, Fukuyama H, Nabatame H, Yamauchi H, Shibasaki H, Yonekura Y. Assessment of benzodiazepine receptors using iodine-123-labeled iomazenil single-photon emission computed tomography in patients with ischemic cerebrovascular disease. A comparison with PET study. *Stroke* 1997; 28:1776–1782.
10. Toyama H, Matsumura K, Nakashima H, Takeda K, Takeuchi A, Koga S, Yoshida T, Ichise M. Characterization of neuronal

damage by iomazenil binding and cerebral blood flow in an ischemic rat model. *Ann Nucl Med* 1998; 12:267–273.
11. Watanabe Y, Nakano T, Yutani K, Nishimura H, Kusuoka H, Nakamura H, Nishimura T. Detection of viable cortical neurons using benzodiazepine receptor imaging after reversible focal ischaemia in rats: comparison with regional cerebral blood flow. *Eur J Nucl Med* 2000; 27:308–313.
12. al-Tikriti MS, Dey HM, Zoghbi SS, Baldwin RM, Zea-Ponce Y, Innis RB. Dual-isotope autoradiographic measurement of regional blood flow and benzodiazepine receptor availability following unilateral middle cerebral artery occlusion. *Eur J Nucl Med* 1994; 21:196–202.
13. Nogawa S, Zhang F, Ross ME, Iadecola C. Cyclo-oxygenase-2 gene expression in neurons contributes to ischemic brain damage. *J Neurosci* 1997; 17:2746–2755.
14. Sairanen T, Ristimaki A, Karjalainen-Lindsberg ML, Paetau A, Kaste M, Lindsberg PJ. Cyclooxygenase-2 is induced globally in infarcted human brain. *Ann Neurol* 1998; 43:738–747.
15. Iadecola C, Forster C, Nogawa S, Clark HB, Ross ME. Cyclooxygenase-2 immunoreactivity in the human brain following cerebral ischemia. *Acta Neuropathol (Berl)* 1999; 98:9–14.
16. Hewett SJ, Uliasz TF, Vidwans AS, Hewett JA. Cyclooxygenase-2 contributes to *N*-methyl-D-asparatate-mediated neuronal cell death in primary cortical cell culture. *J Pharmacol Exp Ther* 2000; 293:417–425.
17. Takedera T, Yumoto H, Tozuka Y, Ohyashiki T. Prostaglandin E(2) induces caspase-dependent apoptosis in rat cortical cells. *Neurosci Lett* 2002; 317:61–64.
18. Gavrieli Y, Sherman Y, Ben-Sasson SA. Identification of programmed cell death in situ via specific labeling of nuclear DNA fragmentation. *J Cell Biol* 1992; 119:493–501.
19. Longa EZ, Weinstein PR, Carlson S, Cummins R. Reversible middle cerebral artery occlusion without craniotomy in rats. *Stroke* 1989; 20:84–91.
20. Minematsu K, Li L, Fisher M, Sotak CH, Davis MA, Fiandaca MS. Diffusion-weighted magnetic resonance imaging:rapid and quantitative detection of focal brain ischemia. *Neurology* 1992; 42:235–240.
21. Kuge Y, Minematsu K, Yamaguchi T, Miyake Y. Nylon monofilament for intraluminal middle cerebral artery occlusion in rats. *Stroke* 1995; 26:1655–1658.
22. Sternberger LA, Sternberger NH. The unlabeled antibody method: comparison of peroxidase- antiperoxidase with avidin-biotin complex by a new method of quantification. *J Histochem Cytochem* 1986; 34:599–605.
23. Tagaya M, Liu K, Copeland B, Seiffert D, Engler R, Garcia JH, Zoppo GJ. DNA scission after focal brain ischemia/temporal differences in two species. *Stroke* 1997; 28:1245–1254.
24. Torizuka K, Uemura K, Toru M, Shinohara Y, Nishimura T, Yonekura Y, Nakagawara J, Matsuda H, Sakai F, Matsuda K, Fukuyama H, Morimoto K. A phase 3 clinical trial of ^{123}I-iomazenil, a new central-type benzodiazepine receptor imaging agent. Part 4. Report on clinical usefulness in diagnosis of cerebrovascular diseases. *Kaku Igaku* 1996; 33:329–344.
25. Moriwaki H, Matsumoto M, Hashikawa K, Oku N, Ishida M, Seike Y, Fukuchi K, Hori M, Nishimura T. Iodine-123-iomazenil and iodine-123-iodoamphetamine SPECT in major cerebral artery occlusive disease. *J Nucl Med* 1998; 39:1348–1353.
26. Matsuoka Y, Okazaki M, Zhao H, Asai S, Ishikawa K, Kitamura Y. Phosphorylation of c-Jun and its localization with heme oxygenase-1 and cyclooxygenase-2 in CA1 pyramidal neurons after transient forebrain ischemia. *J Cereb Blood Flow Metab* 1999; 19:1247–1255.
27. Heiss WD, Grond M, Thiel A, Ghaemi M, Sobesky J, Bauer B, Wienhard K. Permanent cortical damage detected by flumazenil positron emission tomography in acute stroke. *Stroke* 1998; 29:454–461.
28. Heiss WD, Kracht L, Grond M, Rudolf J, Bauer B, Wienhard K, Pawlik G. Early [^{11}C]flumazenil/H_2O positron emission tomography predicts irreversible ischemic cortical damage in stroke patients receiving acute thrombolytic therapy. *Stroke* 2000; 31:366–369.

HDL_3 Induces Cyclooxygenase-2 Expression and Prostacyclin Release in Human Endothelial Cells Via a p38 MAPK/CRE-Dependent Pathway: Effects on COX-2/PGI-Synthase Coupling

G.D. Norata, E. Callegari, H. Inoue, A.L. Catapano

Objective—In endothelial cells, cyclooxygenase-1 (COX-1) and COX-2 both contribute to prostacyclin production. Recent findings suggest that COX-2 contributes significantly to systemic prostacyclin synthesis in humans; whether COX-2 inhibition is related to an increased cardiovascular risk is undergoing debate. HDL have been shown to increase prostacyclin synthesis, thus in the present study we investigated the molecular mechanisms involved in this effect in endothelial cells.

Methods and Results—HDL_3 (30 μg/mL) induced COX-2 expression in a time- and dose-dependent manner. COX-2 was found mainly in the perinuclear area where it co-localizes with PGI synthase. Transient transfection experiments showed that CRE is required for HDL-induced COX-2 transcription, and we demonstrated that p38 MAPK activation by HDL_3 is involved in COX-2 mRNA transcription and stabilization. As a consequence of COX-2-induction by HDL_3 prostacyclin production increased, incubation with a COX-2 selective inhibitor blocked this effect. Moreover, HDL_3 increased caveolin-1 phosphorylation, thus promoting PGI-synthase shuttling from the membrane to the perinuclear area.

Conclusion—We conclude that in endothelial cells, HDL modulate COX-2/PGI-S activity via both p38 MAPK-dependent COX-2 mRNA stability and transcription and both caveolin-1–dependent PGI-synthase shuttling and COX-2 coupling. The understanding of these mechanisms may provide new insights into the antiatherogenic role of HDL. (***Arterioscler Thromb Vasc Biol.* 2004;24:1-8.**)

Key Words: HDL ■ cyclooxygenase-2 ■ p38 MAPK ■ prostacyclin ■ caveolin-1

High-density lipoprotein (HDL) protects from atherosclerotic vascular disease.[1] Beyond reverse cholesterol transport, HDL particles posses several anti-atherosclerotic effects,[2] including the induction of prostacyclin (PGI_2), a strong vasorelaxant[3] that acts also as an inhibitor of platelet and leukocyte activation.[4] The stimulatory effect on PGI_2 depends mainly on the supply by HDL of endothelial cells with arachidonic acid.[3] The rate-limiting step in the conversion of the arachidonic acid to eicosanoids is the activity of cyclooxygenase (COX).[4] Two major forms of COX, COX-1 and COX-2, have been identified.[5] Although COX-1 is constitutively expressed in most cell types, COX-2 is induced by various growth factors and cytokines.[6,7] Recent findings suggest that COX-2 contributes significantly for PGI_2 synthesis in endothelial cells,[8,9] whereas COX-1 is mainly involved in TXA_2 synthesis by platelets.[8,9] Whether COX-2 inhibition is useful as related to an increase of cardiovascular risk is uncertain.[10] HDL induces COX-2 expression in rabbit smooth muscle cells[11] and cooperates with TNF-alpha to elicit this effect,[12] the molecular mechanisms involved, however, are unclear. COX-2 expression is modulated by growth factors and cytokines via mitogen-activated protein kinase (MAPKs) cascade.[13,14] Once activated, the MAPKs may modulate the activity of several transcription factors such as CREB, NFAT, AP-1, and NF-KB,[15–17] which are involved in COX-2 expression.[18–21]

In the present study, we investigated the molecular mechanisms involved in the effect of HDL_3 on COX-2 expression and eicosanoid production in cultured human endothelial cells.

Methods

HDL_3 (dose 1.125 to 1.21 g/mL) was isolated from human plasma and protein content was determined as described.[22] HDL_3 was used within 6 hours from isolation. No LPS contamination was detected as assessed by the endotoxin kit (Sigma, Italy).

Received December 21, 2003; revision accepted February 12, 2004.

From the Department of Pharmacological Sciences (G.D.N., E.C., A.L.C.), University of Milan, Italy; the Department of Pharmacology (H.I.), National Cardiovascular Centre Research Institute, Osaka, Japan; and the Centro per lo Studio e la Prevenzione delle Vasculopatie Periferiche (A.L.C.), Ospedale Bassini, Cinisello Balsamo, Italy.

Correspondence to Prof. Alberico L. Catapano, Department of Pharmacological Sciences, Via Balzaretti, 9 20133 Milano, Italy. E-mail Alberico.Catapano@unimi.it

Arterioscler Thromb Vasc Biol. is available at http://www.atvbaha.org

DOI: 10.1161/01.ATV.zhq0504.1403

HUVECs were isolated and cultured as described.[23] In all experiments, cells were preincubated with serum-free medium for 6 hours,[22-24] then HDL_3 was added.

The antibodies to phospho-p38 MAPK, phospho-p44/42 MAPK, phospho-IkB-alpha, phospho-CREB, and phospho-caveolin-1 were from New England Biolabs (Germany). COX-1, COX-2, and PGI and PGE synthase (PGIS, mPGES-1) monoclonal antibodies were from Cayman (USA). β-Actin antibody was from Sigma. Secondary antibodies were from Biorad (Italy). Western blotting analysis was performed as described;[23] all antibodies were diluted 1:1000, except β-actin (1:10000).

The MEK inhibitor, U0126 (New England Biolabs), and the p38 MAPK inhibitor SB203580 (Sigma) were used at a final concentration of 10 μmol/L and 1 μmol/L, respectively. Indomethacin heptyl ester (Cayman), a selective COX-2 inhibitor,[25] was used at 0.1 μmol/L.

Immunocytochemistry

Cells were cultured on coverslips in 24-well plates. Fixed cells[23] were incubated with a monoclonal antibody for COX-1 or COX-2 (1:50) overnight at 4°C, followed by incubation with anti-mouse IgG FITC-conjugated (1:100, RD, Italy) for 30′, then propidium iodide (2,5 μg/mL) was added for 30′. For the studies of COX-2 co-localization with PGI-S, mPGES-1 and phospho-caveolin-1 fixed cells were incubated overnight with the antibody, followed by incubation with anti IgG FITC-conjugated (30′), anti-COX-2 phycoerythrin-labeled for 1 hour, and TOPRO 3 (Molecular Probes) (1:500) for 15′. The coverslips were analyzed with a confocal microscope (Nikon Eclipse TE 2000-S; Radiance 2100 Biorad) at 600× magnifications. Sixty sections were captured (0.01 μm each) and a three-dimensional reconstruction was obtained using the software Image ProPlace 4.5 (Media Cybernetics, USA).

Real-Time Quantitative Reverse-Transcriptase Polymerase Chain Reaction

Total RNA was extracted and underwent reverse transcription as described.[22,24] Three μL of cDNA were amplified by real-time quantitative polymerase chain reaction (PCR) with 1× Syber green universal PCR mastermix (Biorad). The specificity of the Syber green fluorescence was tested by plotting fluorescence as a function of temperature to generate a melting curve of the amplicon. The melting peaks of the amplicons were as expected (not shown). The primers used, the amplicon size, and the melting temperature are indicated in online Table I (available online at http://atvb.ahajournals.org). Each sample was analyzed in duplicate using the IQ™-Cycler (Biorad). The PCR amplification was related to a standard curve ranging from 10^{-11} M to 10^{-14} M.

Transcription Assay

The construction of various reporter vectors for the human COX-2 gene has been described previously.[20,21] Transfection experiments were first performed using HUVECs and EAhy 926 cells; however, the efficiencies reached were very low, with a high degree of cytotoxicity (data not shown). Because human COX-2 promoter regulation is similar in a wide number of cell types,[26-28] we performed transfection experiments in CHO cells, a cell line widely used for studies involving the effects of HDL in vitro.[29,30] CHO cells were transiently transfected with COX-2 (nucleotide −327/+59), the NF-kB mutated site (KBM), or the CRE mutated site (CRM) luciferase reporter vectors using lipofectamine (Invitrogen, Italy) according to the manufacturer instructions. Luciferase activity was determined and normalized for the cellular protein concentration.[21]

Detection of Prostaglandin Release by Competitive Enzyme Immunoassay

Competitive enzyme immunoassay kits for 6-keto $PGF_1\alpha$, TXB_2 and PGE_2 were from Cayman. HUVECs were exposed to HDL_3 (30 μg/mL) for 6 hours, washed twice with PBS, and then incubated for 30 minutes with exogenous AA (10 μmol/L); 50 μL for each sample were processed for prostaglandin release according to the manufacturer instructions.

Statistical Analysis

Statistical analysis was performed by ANOVA with the use of Statsoft Statistica Package.

Results

HDL_3 Induces COX-2 Expression in HUVECs

COX-2 protein was expressed at low levels in unstimulated cells and was strongly induced 2 hours after exposure to HDL_3 (30 μg/mL). In preliminary experiments, this concentration maximally induced COX-2 expression and no further increase was observed up to 600 μg/mL of HDL_3. The induction was maximal after 4 hours and begun to decrease after 8 hours (Figure 1a). In unstimulated cells, COX-2 expression remained low at all time points (data not shown). Under the same experimental conditions, HDL_3 did not affect COX-1 expression (Figure 1a). These findings were confirmed by immunocytochemistry. COX-2 expression increased after 4 hours in cells incubated with HDL_3 without changes of COX-1 expression (Figure 1b). On three-dimensional reconstruction, COX-2 localized in the perinuclear area and in the cytoplasm[31] (Figure 1c).

Effects of HDL_3 on Intracellular Kinase Pathways and on COX-2 Promoter Activity

HDL_3 activated ERK1/2 and p38 MAPK, with a the peak of phosphorylation reached after 5 to 10 minutes of incubation (Figure 2). Several transcription factors are activated through MAPK-dependent pathways.[17-19] HDL_3 activated CREB, with a peak of activity at 10 to 20 minutes (Figure 2), in agreement with the observation that both ERK1/2 and p38 MAPK activate CREB via p90RSK or via MSK-1, respectively. Ik-B alpha phosphorylation results in the release and nuclear translocation of active NF-kB.[17] Under our experimental conditions, a basal level of phosphorylation of Ik-B alpha was present, and only a minimal effect on phosphorylation was observed after 5 and 10 minutes of incubation with HDL_3 (Figure 2). The human COX-2 promoter region (−327/+59) contains the NF-kB, the NF-IL6, and the CRE sites.[20,21] Transient transfection assay showed that HDL_3 induced promoter activity by 2.96±0.03-fold, whereas LPS (1 μg/mL), a positive control, induced promoter activity by 4.24±0.02-fold ($P<0.01$ for both versus control) (Figure 3). The promoter activity of the plasmid carrying the mutation at the NF-kB site was 1.87±0.12 fold in HDL_3 incubated cells ($P<0,01$) and 0.93±0.09 fold in LPS-treated cells, whereas that of the mutant carrying the mutation at the CRE site was 1.15±0.03-fold in HDL_3-treated cells and 1.26±0.16-fold in LPS treated cells (Figure 3; P=NS versus control).

Involvement of p38-MAPK in HDL_3-Induced COX-2 Protein and mRNA Expression and Stabilization

Cells were preincubated with the MEK1 inhibitor U 0126 (25 μmol/L) or the p38 MAPK inhibitor SB 203580 (1 μmol/L) for 1 hour. HDL_3 (30 μg/mL) were added for 2 and 4 hours to evaluate COX-2 mRNA and protein expression. U0126 did not affect HDL_3-induced COX-2 expression.

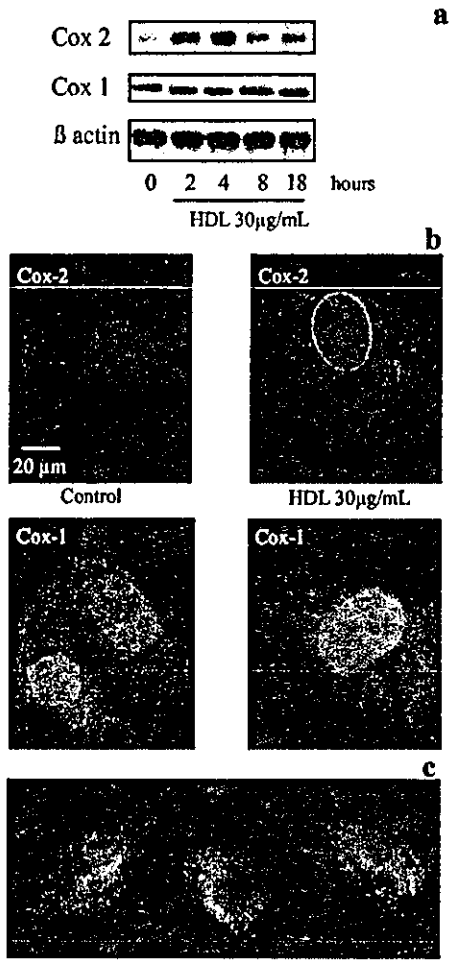

Figure 1. Time dependency of COX-1 and COX-2 expression as detected by Western immunoblotting (a) and indirect immunofluorescence (b) in HUVEC incubated with HDL_3 for 4 hours (30 µg/mL). (The green signal represents COX-1 or COX-2, whereas the red one is the nuclear staining with propidium iodide). A three-dimensional reconstruction showing that COX-2 localizes mainly in the perinuclear cytoplasm is shown (c). Three different projections are shown. The results are representative of 4 separate experiments.

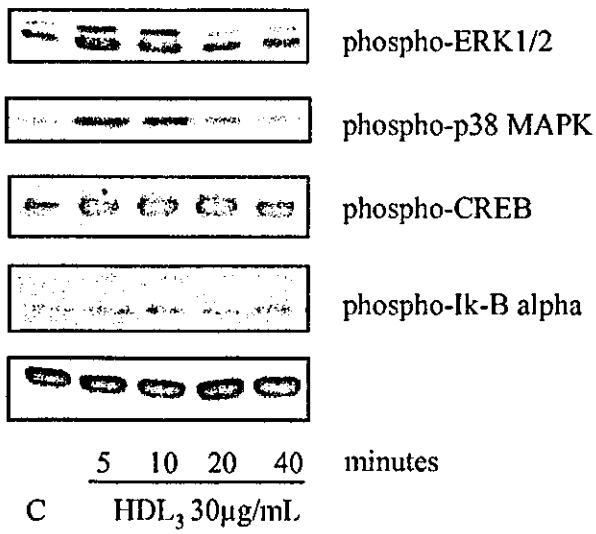

Figure 2. Time-dependent phosphorylation of ERK1/2, P38 MAPK, CREB, and Ik-B alpha after incubation of endothelial cells with HDL_3. HUVEC were incubated from 5 minutes up to 40 minutes with HDL_3 (30 µg/mL). The results are representative of 4 experiments.

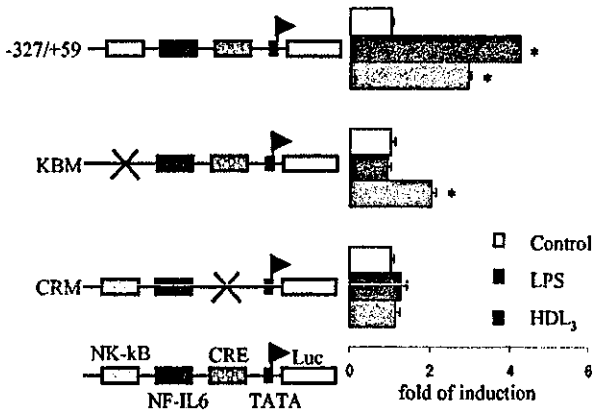

Figure 3. Identification of the regions responsible for HDL_3-induced promoter activity of the human COX-2 gene. The 5′-flanking region of the human COX-2 gene with site-specific mutations are represented schematically on the left. After transfection, CHO cells were incubated for 6 hours with LPS (1 μg/mL), used as positive control, and with HDL_3 (30 μg/mL). The results are presented as relative luciferase activity normalized to cellular protein content. Each experiment was performed in triplicate. *$P<0.01$ versus control.

$SB203580$ strongly inhibited HDL_3-mediated COX-2 mRNA and protein expression (Figure 4). Because p38 MAPK stabilizes COX-2 mRNA,[32] we investigated whether HDL_3 possesses this effect. To asses the stability of COX-2 mRNA in HUVEC, actinomycin D (2 μg/mL) was added to cells after 2 hours of HDL_3 incubation and COX-2 mRNA levels were measured up to 60 minutes (Figure 4). Simultaneous addition of SB203580 (1 μmol/L) and actinomycin D to the cells after a 2-hour stimulation with HDL_3 resulted in a more rapid decrease in COX-2 mRNA levels, suggesting mRNA stabilizing effect by p38 MAPK activity.

Effects of HDL_3 on Eicosanoid Production

The effects of HDL_3 on eicosanoids production were assessed in HUVECs exposed to 30 μg/mL of lipoproteins for 6 hours, followed by 30 minutes of incubation with exogenous AA (10 μmol/L).[11] In control cells, the production of 6-keto $PGF_1\alpha$ (PGI_2 main metabolite) was 73.14±6.79 pg/mg of

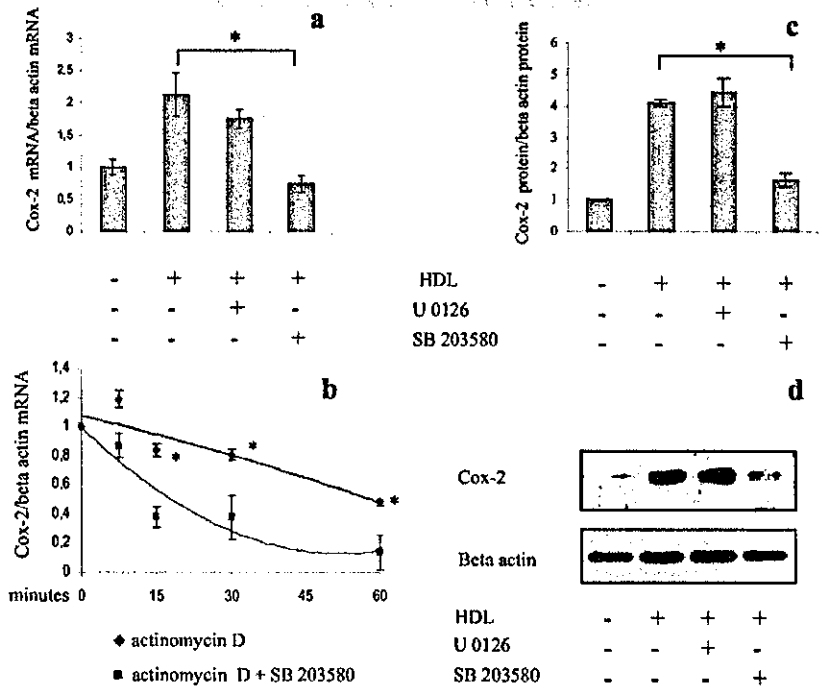

Figure 4. Involvement of p38 MAPK pathway in COX-2 mRNA (a and b) and protein expression induced by HDL_3 (c and d). HUVECs were incubated for 2 hours (for mRNA detection) and 4 hours (for protein detection) with HDL_3 (30 μg/mL) alone or in the presence of U0126 (25 μmol/L) or of SB203580 (1 μmol/L). a, COX-2 mRNA expression was assessed with real-time quantitative PCR; the target sequence was normalized to the beta actin content. b, Inhibition of p38 MAPK destabilizes COX-2 mRNA expression induced by HDL_3. HUVECs were incubated for 2 hours with HDL_3 (30 μg/mL), then actinomycin D alone or actinomycin D plus SB203580 were added (time 0). COX-2 mRNA levels were measured using real-time quantitative PCR from time 0 minutes up to 60 minutes. Data are mean±SD of 4 separate experiments. *$P<0.01$. c and d, COX-2 protein expression was assessed by immunoblotting. c, The results are mean±SD of 4 separate experiments and are normalized for beta actin content. *$P<0.01$.

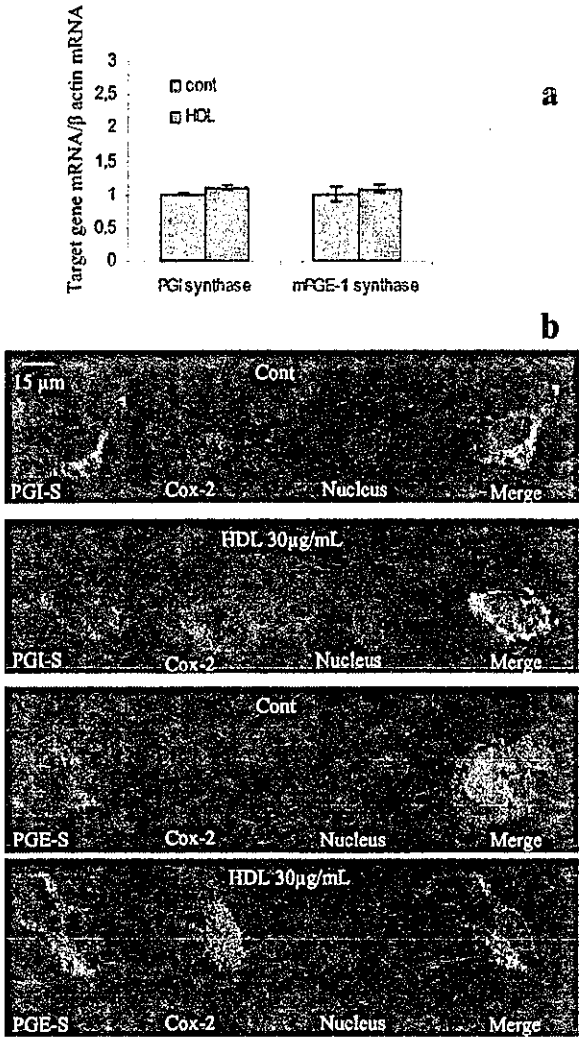

Figure 5. Effects of HDL_3 on PGI-S and PGE-S mRNA expression and cellular localization. a, HUVECs were incubated for 2 hours with HDL_3 (30 µg/mL) and COX-2 mRNA levels were measured using quantitative real-time PCR. Data are mean±SD of 4 separate experiments. b, cellular localization of COX-2 and PGI-S or PGE-S. The green signal is for PGI-S or PGE-S, the red signal is for COX-2, and the blue signal is the staining for the nucleus. The results are representative of 4 experiments.

cellular protein. Incubation of endothelial cells with HDL_3 increased 6-keto $PGF_1\alpha$ production to 113.38±2.54 pg/mg of cellular protein ($P<0,01$) (Table II, available online at http://atvb.ahajournals.org). In the presence of 0.1 µmol/L indomethacin eptyl ester, a selective COX-2 inhibitor,[25] HDL_3-induced 6-keto $PGF_1\alpha$ production was reduced to 77.95±10.19 pg/mg of cellular protein and PGE_2 resulted in 74.10±3.45 pg/mg of cellular protein and was not affected by HDL_3 incubation.

Effects of HDL_3 on PGI Synthase Expression and Cellular Localization

As HDL_3 induces COX-2 expression and increases PGI_2 release, we investigated whether HDL_3 can affect PGI-S or mPGES-1 expression. HDL incubation did not change PGI-S or mPGES-1 expression (1.10±0.2-fold and 1.07±0.5-fold versus control cells, respectively) (Figure 5a). Furthermore, in HDL-treated cells, PGI-S co-localized with COX-2 while mPGES-1 showed a different subcellular distribution (Figure 5b).

PGI-S resides in caveolae in resting cells.[33] Caveolin-1 is the main protein of caveolae, and when phosphorylated[34] it moves into the cytoplasm,[34,35] shuttling PGI-S in the perinuclear area where it couples to COX-2,[35] thus increasing prostacyclin synthesis. We investigated, therefore, whether HDL can influence caveolin-1 phosphorylation and shuttling in the perinuclear space. After 4 hours of incubation, HDL increased caveolin-1 phosphorylation (Figure 6a), mainly in the area surrounding the nucleus (Figure 6b). Moreover, a three-dimensional reconstruction shows that phosphorylated caveolin-1 localizes near COX-2 in the perinuclear area of HDL-treated cells (Figure 6c), where PGI-S is also located (Figure 6d).

Discussion

The major finding of this study is that HDL_3 induces COX-2 expression and PGI_2 release in human endothelial cells via p38 MAPK activation. The activation of this signaling pathway promotes COX-2 mRNA transcription and stabilization.

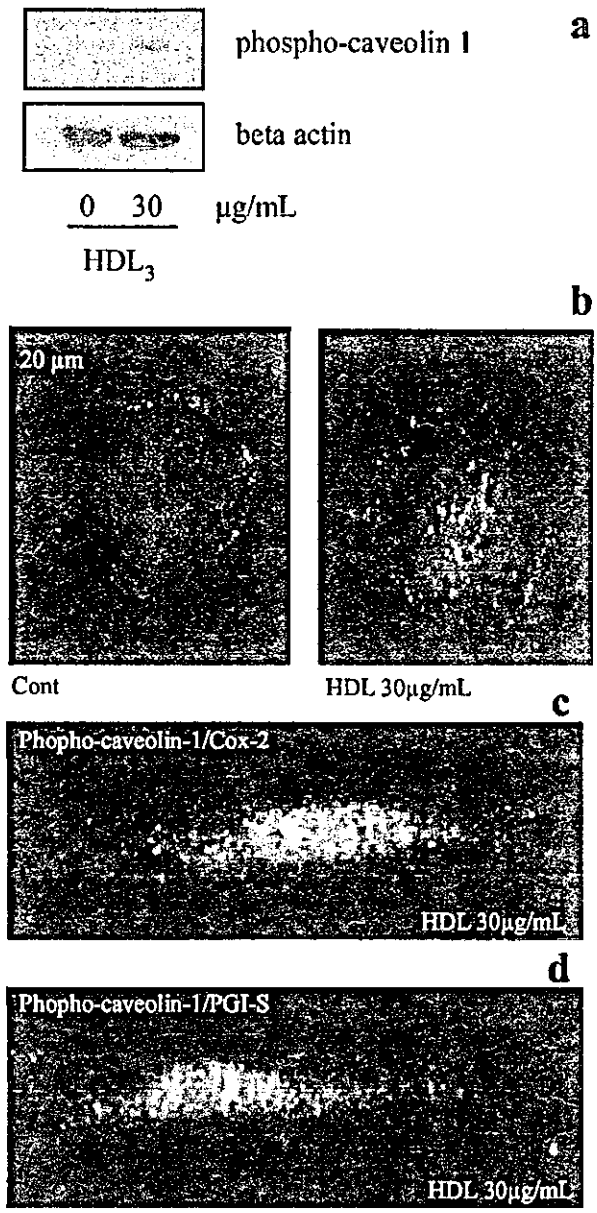

Figure 6. Effects of HDL_3 on caveolin-1 phosphorylation and cellular localization. a, HUVECs were incubated for 4 hours with HDL_3 (30 µg/mL) and phospho-caveolin-1 levels were determined by Western blotting. b, cellular localization of phospho-caveolin-1. The green signal is for phospho-caveolin-1, the blue is staining for the nucleus. c, Cellular localization of phospho-caveolin-1 and COX-2 (transversal projection). The green signal is for phospho-caveolin-1, the red signal is for COX-2, and the blue signal is the nucleus. d, Cellular localization of phospho-caveolin-1 and PGI-S (transversal projection). The green signal is for phospho-caveolin-1, the red signal is for PGI-S, and the blue signal is the nucleus. The results are representative of 4 experiments.

On incubation of cells with HDL_3, COX-2 protein localized mainly in the perinuclear area, in agreement with previous findings showing that COX-2 accumulation near the nuclear envelope and in the cytoplasm is required for the increase in COX-2–mediated prostanoid synthesis in vascular endothelial cells.[35,36] This effect is specific for COX-2; in fact, COX-1 was mainly localized in the cytoplasm and was not modulated by HDL_3; moreover, PGI_2 synthesis was downregulated by a specific COX-2 inhibitor.

The molecular mechanisms by which HDL_3 induces COX-2 are unknown. Here we show that HDL_3 activates 2 of the major kinases pathways involved in COX-2 gene transcription: ERK1/2 and p38 MAPK.[13,14] HDL can activate ERK1/2 via cell surface S1P receptor in astroglial cells.[37] However, the possibility that MAPK activation results from plasma membrane cholesterol depletion cannot be excluded.[38] In support of this hypothesis, Smith et al[39] showed that increasing concentration of LDL or free cholesterol decreases COX-2 expression and PGI_2 synthesis. As HDL triggers the release of cholesterol from cells,[2] our observation suggests that cellular cholesterol balance plays an important role in determining COX-2 levels.

HDL_3 also activates CREB in a time-dependent fashion, CREB binds to CRE, which serves as an anchor for P300 interaction with upstream transactivators and downstream transcription machinery,[40] thus suggesting that CRE plays a relevant role in COX-2 induction by a number of stimuli.[40] Using transient transfection experiments, we demonstrated that mutation in CRE abrogated the luciferase activity induced by HDL_3, confirming the role of CRE in HDL_3-induced COX-2 gene transcription.

NF-kB has also been suggested to be involved in determining COX-2 gene transcription.[20,21] We show that a mutation in the NF-kB response element abrogates luciferase activity induced by LPS, used as a positive control, while it slightly decreases HDL_3-induced luciferase activity, suggesting a minor role of this pathway in COX-2 induction by HDL_3.

As transcriptional regulation of the COX-2 gene occurs via activation of MAPKs,[13,14] we investigated whether inhibition of ERK1/2 or p38 MAPK pathway affected HDL_3-induced COX-2 mRNA and protein expression. We show that the p38 MAPK pathway is responsible for the induction of COX-2 by HDL_3.

P38 MAPK plays a housekeeping role in maintaining COX-2 mRNA stability[32] via the recognition of the AUUUA motifs present in the 3' untranslated region of COX-2.[41] We therefore studied COX-2 mRNA stability in cells stimulated with HDL_3. Simultaneous addition of actinomycin D and SB203580 to the cells resulted in a more rapid decrease in COX-2 mRNA compared with actinomycin D alone. This represents a new mechanism by which HDL can influence gene expression at a posttranscriptional level and is likely to contribute to the increase of COX-2 protein levels in endothelial cells.

COX-2 has been proposed to exert both an antiatherogenic or a proatherogenic role depending on the eicosanoids produced and the arterial wall cells where it is expressed.[9] Eicosanoids are involved in a variety of physiological processes in atherosclerosis and thrombosis, including leukocyte–endothelial cell adhesion, vasorelaxation, and platelet aggregation.[9] The dominant prostaglandin produced by endothelial cells is PGI_2.[4] PGI_2 is believed to play a protective role in atherothrombosis.[4] COX-2 contributes significantly to systemic PGI_2 synthesis in humans;[42] therefore, it is possible that COX-2 induced in endothelial cells at lesion-protected areas catalyzes the formation of the anti-atherogenic molecule prostacyclin. This may be the case in the presence of HDL_3 that increases PGI_2 release mediated by AA in endothelial cells. This effect is dependent mainly on COX-2 as indomethacin eptyl ester, a specific COX-2 inhibitor, abolished PGI_2 release induced by HDL_3. This observation may also be relevant to the recent observation that COX-2 inhibitors may increase CHD risk.[10] In vitro 30 μg/mL of HDL_3 induces maximally COX-2 expression, and no further increase is observed up to 600 μg/mL (a physiological concentration that constantly bathes arteries in vivo), thus suggesting that low concentrations of HDL are enough to support COX-2 expression, and higher levels may only provide the substrate. Alternatively, the in vitro conditions allow for a better interaction of HDL with cultured endothelial cells as compared with in vivo settings, in which proteoglycans may trap lipoproteins and reduce their availability for interactions with the endothelial cells.

The observation that COX-2 induced by HDL_3 does not increase PGE_2, a proatherogenic eicosanoid, synthesized mainly via COX-2,[12] confirms that COX-2 expression in the arterial wall could play both a proatherogenic or antiatherogenic role, but it is the final eicosanoid produced that is responsible for its proatherogenic or anti-atherogenic properties.

Moreover, HDL_3-induced COX-2 protein co-localizes with PGI-S in endothelial cells, thus suggesting that in this model, once induced, COX-2 can drive prostacyclin synthesis. PGI-S is associated with caveolae[33] and is activated when shuttled from the plasma membrane in the perinuclear area;[35] moreover, disruption of caveolae organization downregulates prostacyclin production and impairs angiogenesis.[43,44] Here we demonstrate that HDL_3 induces caveolin-1 phosphorylation, which shuttles with PGI-S from the plasma membrane to the perinuclear area where it co-localizes with COX-2. Furthermore, the possibility that the abundant increase in COX-2 observed can be related to an increase of prostanoids synthesis other than prostacyclin cannot be excluded.

Also, endothelial nitric oxide synthase, the enzyme responsible for nitric oxide synthesis in the endothelium, localizes in the caveolae.[33,35] Nitric oxide is responsible for several beneficial effects of HDL on endothelial cells,[45] such as helping to maintain endothelial integrity, facilitating vascular relaxation, inhibiting cell adhesion to vascular endothelium, decreasing radical oxygen production, and inhibiting apoptosis.[45] Even if we have not addressed the role of HDL in modulating endothelial nitric oxide synthase shuttling through caveolin-1 phosphorylation, it is conceivable that some of the effects of HDL are mediated via this pathway[46]

In summary, our data suggest that in human endothelial cells, HDL can modulate COX-2 expression via p38 MAPK-dependent COX-2 mRNA transcription and stabilization. Moreover, the HDL-dependent caveolin-1 phosphorylation favors PGI-S shuttling and COX-2 coupling. These data add further insights into the molecular mechanisms involved in the anti-atherogenic activity of HDL.

Acknowledgments

We are grateful to Roberto Zecca for software assistance, to Giulio Simonutti for technical assistance at confocal microscopy, to Fabio Pellegatta, who provided the HUVECs, and to Francesco Cipollone, who provided the anti-mPGES antibody.

References

1. Assmann G, Schulte H, von Eckardstein A, Huang Y. High-density lipoprotein cholesterol as a predictor of coronary heart disease risk. The PROCAM experience and pathophysiological implications for reverse cholesterol transport. *Atherosclerosis*. 1996;124:S11–S20.
2. Nofer JR, Kehrel B, Fobker M, Levkau B, Assmann G, von Eckardstein A. HDL and arteriosclerosis: beyond reverse cholesterol transport. *Atherosclerosis*. 2002;161:1–16.
3. Fleisher LN, Tall AR, Witte LD, Miller RW, Cannon PJ. Stimulation of arterial endothelial cell prostacyclin synthesis by high density lipoproteins. *J Biol Chem*. 1982;257:6653–6655.
4. Thiemermann C. Biosynthesis and interaction of endothelium-derived vasoactive mediators. *Eicosanoids*. 1991;4:187–202.

5. Vane JR, Bakhle Y, Botting R. Cyclooxygenase 1 and 2. *Ann Rev Pharmacol Toxicol.* 1998;38:97–120.
6. Bartlett SR, Sawdy R, Mann GE. Induction of cyclooxygenase-2 expression in human myometrial smooth muscle cells by interleukin-1 beta: involvement of p38 mitogen-activated protein kinase. *J Physiol.* 1999;520:399–406.
7. Lee SH, Soyoola E, Chanmugam P, Hart S, Sun W, Zhong H, Liou S, Simmons D, Hwang D. Selective expression of mitogen-inducible cyclooxygenase in macrophages stimulated with lipopolysaccharide. *J Biol Chem.* 1992;267:25934–25938.
8. Caughey GE, Cleland LG, Penglis PS, Gamble JR, James MJ. Roles of cyclooxygenase (COX)-1 and COX-2 in prostanoid production by human endothelial cells: selective up-regulation of prostacyclin synthesis by COX-2. *J Immunol.* 2001;167:2831–2838.
9. Linton MF, Fazio S. Cyclooxygenase-2 and atherosclerosis. *Curr Opin Lipidol.* 2002;13:497–504.
10. Ray WA, Stein CM, Daugherty JR Hall K, Arbogast PG, Griffin MR. COX-2 selective non-steroidal anti-inflammatory drugs and risk of serious coronary heart disease. *Lancet.* 2002;360:1071–1073.
11. Vinals M, Martinez-Gonzalez J, Badimon L. Regulatory effects of HDL on smooth muscle cell prostacyclin release. *Arterioscler Thromb Vasc Biol.* 1999;19:2405–2411.
12. Cockerill GW, Saklatvala J, Ridley SH, Yarwood H, Miller NE, Oral B, Nithyanathan S, Taylor G, Haskard DO. High-density lipoproteins differentially modulate cytokine-induced expression of E-selectin and cyclooxygenase-2. *Arterioscler Thromb Vasc Biol.* 1999;19:910–917.
13. Guan Z, Buckman SY, Miller BW, Springer LD, Morrison AR. Interleukin-1β-induced cyclooxygenase-2 expression requires activation of both c-Jun NH2-terminal kinase and p38 MAPK signal pathway in rat mesangial cells. *J Biol Chem.* 1998;273:28670–28676.
14. LaPointe MC, Isenovic E. Interleukin-1β regulation of inducible nitric oxide synthase and cyclooxygenase-2 involves the p44/44 and p38 MAPK signalling pathways in cardiac myocytes. *Hypertension.* 1999;33: 276–282.
15. Seger R, Krebs EG. The MAPK signalling cascade. *FASEB J.* 1995;9: 726–735.
16. Hazzalin CA, Mahadevan LC. MAPK-regulated transcription: a continuously variable gene switch? *Nat Rev Mol Cell Biol.* 2002;3:30–40.
17. Schulze-Osthoff K, Ferrari D, Riehemann K, Wesselborg S. Regulation of NF-kappa B activation by MAP kinase cascades. *Immunobiology.* 1997;198:35–49.
18. Tan Y, Rouse J, Zhang A, Cariati S, Cohen P, Comb MJ. FGF and stress regulate CREB and ATF-1 via a pathway involving p38 MAP kinase and MAPKAP kinase-2. *EMBO J.* 1996;15:4629–4642.
19. Xie W, Herschman HR. v-src induces prostaglandin synthase 2 gene expression by activation of the c-Jun N-terminal kinase and the c-Jun transcription factor. *J Biol Chem.* 1995;270:27622–27628.
20. Inoue H, Yokoyama C, Hara S, Tone Y, Tanabe T. Transcriptional regulation of human prostaglandin-endoperoxide synthase-2 gene by lipopolysaccharide and phorbol ester in vascular endothelial cells. Involvement of both nuclear factor for interleukin-6 expression site and cAMP response element. *J Biol Chem.* 1995;270:24965–24971.
21. Inoue H, Umesono K, Nishimori T, Hirata Y, Tanabe T. Glucocorticoid-mediated suppression of the promoter activity on the cyclooxygenase-2 gene is modulated by expression of its receptor in vascular endothelial cells. *Biochem Biophys Res Comm.* 1999;254:292–298.
22. Norata GD, Pellegatta F, Hamsten A, Catapano AL, Eriksson P. Effects of high density lipoprotein subfraction 3 on the expression of matrix-degrading proteases in human endothelial cells. *Int J Mol Med.* 2003;12: 73–78.
23. Norata GD, Pirillo A, Callegari E, Hamsten A, Catapano AL, Eriksson P. Gene expression and intracellular pathways involved in endothelial dysfunction induced by VLDL and oxidised VLDL. *Cardiovasc Res.* 2003; 59:169–180.
24. Norata GD, Bjork H, Hamsten A, Catapano AL, Eriksson P. High density lipoprotein decrease ADAMTs1 expression induced by LPS and TNFα in human endothelial cells. *Matrix Biology.* 2004;in press.
25. Kalgutkar AS, Marnett AB, Crews BC, Remmel RP, Marnett LJ. Ester and amide derivatives of the non-steroidal anti-inflammatory drug, indomethacin, as selective cyclooxygenase-2 inhibitors. *J Med Chem.* 2000; 43:2860–2870.
26. Singer CA, Baker KJ, McCaffrey A, AuCoin DP, Dechert MA, Gerthoffer WT. P38 MAPK and NF-{kappa}B Mediate COX-2 Expression in Human Airway Myocytes. *Am J Physiol Lung Cell Mol Physiol.* 2003;285:L1087–L1098.
27. Loudon JA, Elliott CL, Hills F, Bennett PR. Progesterone represses interleukin-8 and cyclo-oxygenase-2 in human lower segment fibroblast cells and amnion epithelial cells. *Biol Reprod.* 2003;69:331–337.
28. Tamura M, Sebastian S, Yang S, Gurates B, Fang Z, Okamura K, Bulun SE. Induction of cyclooxygenase-2 in human endometrial stromal cells by malignant endometrial epithelial cells: evidence for the involvement of extracellularly regulated kinases and CCAAT/enhancer binding proteins. *J Mol Endocrinol.* 2003;31:95–104.
29. Baez JM, Barbour SE, Cohen DE. Phosphatidylcholine transfer protein promotes apolipoprotein A-I-mediated lipid efflux in Chinese hamster ovary cells. *J Biol Chem.* 2002;277:6198–6206.
30. Ioka RX, Kang MJ, Kamiyama S, Kim DH, Magoori K, Kamataki A, Ito Y, Takei YA, Sasaki M, Suzuki T, Sasano H, Takahashi S, Sakai J, Fujino T, Yamamoto TT. Expression cloning and characterization of a novel glycosylphosphatidylinositol-anchored high density lipoprotein-binding protein, GPI-HBP1. *J Biol Chem.* 2003;278:7344–7349.
31. Parfenova H, Parfenov VN, Shlopov BV, Levine V, Falkos S, Pourcyrous M, Leffler CW. Dynamics of nuclear localization sites for COX-2 in vascular endothelial cells. *Am J Physiol Cell Physiol.* 2001;281: C166–C178.
32. Dean JLE, Brook M, Clark AR, Saklatvala J. P38 MAPK regulates cyclooxygenase-2 mRNA stability and transcription in lipopolysaccharide-treated human monocytes. *J Biol Chem.* 1999;274:264–269.
33. Frank PG, Woodman SE, Park DS, Lisanti MP. Caveolin, caveolae, and endothelial cell function. *Arterioscler Thromb Vasc Biol.* 2003;23: 1161–1168.
34. Nomura R, Fujimoto T. Tyrosine-phosphorylated caveolin-1: immunolocalization and molecular characterization. *Mol Biol Cell.* 1999;10: 975–986.
35. Spisni E, Bianco MC, Griffoni C, Toni M, D'Angelo R, Santi S, Riccio M, Tomasi V. Mechanosensing role of caveolae and caveolar constituents in human endothelial cells. *J Cell Physiol.* 2003;197:198–204.
36. Lim H, Dey SK. A Novel Pathway of Prostacyclin Signalling-Hanging Out with Nuclear Receptors. *Endocrinology.* 2002;143:3207–3210.
37. Kimura T, Sato K, Malchinkhuu E, Tomura H, Tamama K, Kuwabara A, Murakami M, Okajima F. High-density lipoprotein stimulates endothelial cell migration and survival through sphingosine 1-phosphate and its receptors. *Arterioscler Thromb Vasc Biol.* 2003;23:1283–1288.
38. Chen X, Resh MD. Activation of mitogen-activated protein kinase by membrane-targeted Raf chimeras is independent of raft localization. *J Biol Chem.* 2001;34617–34623.
39. Smith LH, Boutaud O, Breyer M Morrow JD, Oates JA, Vaughan DE. Cyclooxygenase-2-Dependent Prostacyclin Formation Is Regulated by Low Density Lipoprotein Cholesterol In Vitro. *Arterioscler Thromb Vasc Biol.* 2002;22:983–988.
40. Schroer K, Zhu Y, Saunders MA, Deng WG, Xu XM, Meyer-Kirchrath J, Wu KK. Obligatory role of cyclic adenosine monophosphate response element in cyclooxygenase-2 promoter induction and feedback regulation by inflammatory mediators. *Circulation.* 2002;105:2760–2765.
41. Inoue H, Taba Y, Miwa Y, Yokota C, Miyagi M, Sasaguri T. Transcriptional and posttranscriptional regulation of cyclooxygenase-2 expression by fluid shear stress in vascular endothelial cells. *Arterioscler Thromb Vasc Biol.* 2002;22:1415–1420.
42. McAdam BF, Catella-Lawson F, Mardini IA, Kapoor S, Lawson JA, FitzGerald GA. Systemic biosynthesis of prostacyclin by cyclooxygenase (COX)-2: The human pharmacology of selective inhibitors of COX-2. *Proc Natl Acad Sci U S A.* 1999;96:272–277.
43. Griffoni C, Spisni E, Santi S, Riccio M, Guarnieri T, Tomasi V. Knockdown of caveolin-1 by antisense oligonucleotides impairs angiogenesis in vitro and in vivo. *Biochem Biophys Res Commun.* 2000;276: 756–761.
44. Spisni E, Griffoni C, Santi S, Riccio M, Marulli R, Bartolini G, Toni M, Ullrich V, Tomasi V. Colocalization of PGI-S and caveolin-1 in endothelial cells and new role for prostacyclin in angiogenesis. *Exp Cell Res.* 2001;266:31–43.
45. Calabresi L, Gomaraschi M, Franceschini G. Endothelial protection by HDL. From bench to beside. *Arterioscler Thromb Vasc Biol.* 2003;23: 1724–1731.
46. Uittenbogaard A, Shaul PW, Yuhanna IS, Blair A, Smart EJ. HDL prevents Ox-LDL-induced inhibition of eNOS localization and activation in caveolae. *J Biol Chem.* 2000;275:11278–11283.

0026-895X/04/6603-667-674$20.00
MOLECULAR PHARMACOLOGY
Copyright © 2004 The American Society for Pharmacology and Experimental Therapeutics
Mol Pharmacol 66:667–674, 2004

Vol. 66, No. 3
2626/1172525
Printed in U.S.A.

γ-Mangostin Inhibits Inhibitor-κB Kinase Activity and Decreases Lipopolysaccharide-Induced Cyclooxygenase-2 Gene Expression in C6 Rat Glioma Cells

Keigo Nakatani,[1] Tohru Yamakuni, Nobuhiko Kondo, Tsutomu Arakawa, Kenji Oosawa, Susumu Shimura, Hiroyasu Inoue, and Yasushi Ohizumi

Department of Pharmaceutical Molecular Biology, Graduate School of Pharmaceutical Sciences, Tohoku University, Sendai, Japan (K.N., T.Y., N.K., Y.O.); Central Laboratory, Lotte Co., Ltd., Saitama, Japan (T.A., K.O., S.S.); and Department of Pharmacology, National Cardiovascular Center Research Institute, Osaka, Japan (H.I.)

Received May 11, 2004; accepted June 18, 2004

ABSTRACT

We investigated the effect of γ-mangostin purified from the fruit hull of the medicinal plant *Garcinia mangostana* on spontaneous prostaglandin E_2 (PGE_2) release and inducible cyclooxygenase 2 (COX-2) gene expression in C6 rat glioma cells. An 18-h treatment with γ-mangostin potently inhibited spontaneous PGE_2 release in a concentration-dependent manner with the IC_{50} value of approximately 2 μM, without affecting the cell viability even at 30 μM. By immunoblotting and reverse-transcription polymerase chain reaction, we showed that γ-mangostin concentration-dependently inhibited lipopolysaccharide (LPS)-induced expression of COX-2 protein and its mRNA, but not those of constitutive COX-1 cyclooxygenase. Because LPS is known to stimulate inhibitor κB (IκB) kinase (IKK)-mediated phosphorylation of IκB followed by its degradation, which in turn induces nuclear factor (NF)-κB nuclear translocation leading to transcriptional activation of COX-2 gene, the effect of γ-mangostin on the IKK/IκB cascade controlling the NF-κB activation was examined. An in vitro IKK assay using IKK protein immunoprecipitated from C6 cell extract showed that this compound inhibited IKK activity in a concentration-dependent manner, with the IC_{50} value of approximately 10 μM. Consistently γ-mangostin was also observed to decrease the LPS-induced IκB degradation and phosphorylation in a concentration-dependent manner, as assayed by immunoblotting. Furthermore, luciferase reporter assays showed that γ-mangostin reduced the LPS-inducible activation of NF-κB–and human COX-2 gene promoter region-dependent transcription. γ-Mangostin also inhibited rat carrageenan-induced paw edema. These results suggest that γ-mangostin directly inhibits IKK activity and thereby prevents COX-2 gene transcription, an NF-κB target gene, probably to decrease the inflammatory agent-stimulated PGE_2 production in vivo, and is a new useful lead compound for anti-inflammatory drug development.

Prostaglandins (PGs), arachidonic acid (AA) metabolites of the cyclooxygenase (COX) pathway, are major mediators in the regulation of inflammation and immune function (Smith et al., 2000). In the brain, the prostaglandin E_2 (PGE_2) is the most abundant PG. PGE_2 levels are very low or undetectable in normal conditions but can rise in response to inflammatory processes, multiple sclerosis, and AIDS-associated dementia (Fretland, 1992; Griffin et al., 1994). High levels of PGE_2 can modulate the activities of multiple cell types, including neurons, glial, and endothelial cells, as well as microglia/macrophage and lymphocyte functions during inflammatory and immune processes (Weissmann, 1993). Astrocytes are a known important source of PGE_2 in the CNS (Katsuura et al., 1989). Their ability to produce PGE_2 upon stimulation with interleukin (IL)-1β, tumor necrosis factor-α (TNF-α), or bacterial wall protein lipopolysaccharide (LPS) has been extensively documented (Fontana et al., 1982; Mollace et al., 1998; Molina-Holgado et al., 2000).

Cyclooxygenase (COX) is well known to be responsible for PG production and the rate-limiting enzymes. This enzyme

This work was partly supported by a Grant-in-Aid for Scientific Research from the Ministry of Education, Science, Sport and Culture of Japan.

[1] Current address: Pfizer Global Research and Development, Nagoya Laboratories, Aichi, Japan.

Article, publication date, and citation information can be found at http://molpharm.aspetjournals.org.
doi:10.1124/mol.104.002626.

ABBREVIATIONS: PG, prostaglandin; AA, arachidonic acid; COX, cyclooxygenase; COX-1, constitutive cyclooxygenase; COX-2, inducible cyclooxygenase; PGE_2, prostaglandin E_2; LPS, lipopolysaccharide; IκB, inhibitor κB; IKK, inhibitor κB kinase; CNS, central nervous system; IL, interleukin; TNF-α, tumor necrosis factor-α; NF-κB, nuclear factor-κB; MTT, 3-(4,5-dimethylthiazol-2-yl)-2,5-diphenyltetrazolium; RT, reverse transcription; PCR, polymerase chain reaction; PAGE, polyacrylamide gel electrophoresis; ODS, octadecylsilyl; HPLC, high-performance liquid chromatography; DMSO, dimethyl sulfoxide; NS398, *N*-[2-(cyclohexyloxyl)-4-nitrophenyl]-methane sulfonamide.

exists as two isoforms, namely constitutive COX (COX-1) and inducible COX (COX-2). COX-2 gene is an early-inducible gene in response to many inflammatory cytokines, including IL-1, TNF-α, and LPS. COX-2 gene expression is controlled at the transcriptional and/or the post-transcriptional levels (Dixon et al., 2000). The promoter regions of COX-2 gene of rat, human, and mouse have been extensively analyzed (Sirois et al., 1993; Appleby et al., 1994; Kosaka et al., 1994; Inoue et al., 1995) and have been shown to contain potential binding sites for various transcriptional factors, some of which have been demonstrated to be indeed functional (Goppelt-Struebe, 1995). For example, activation of nuclear factor-κB (NF-κB) has been reported recently to actually participate in the transcriptional activation of COX-2 gene induced by IL-1 (Newton et al., 1997), TNF-α (Yamamoto et al., 1995), and LPS (Inoue and Tanabe, 1998). Furthermore, the LPS-induced activation of COX-2 gene evidently has been shown to be mediated by inhibitor κB (IκB) kinase (IKK), which specifically catalyzes IκB phosphorylation followed by its degradation and the subsequent NF-κB nuclear translocation, leading to a stimulation of the *cis*-acting κB element-mediated transcription (Griseavage et al., 1996).

Because the fruit hull of mangosteen, *Garcinia mangostana*, has been used for many years as traditional medicine for the treatment of skin infection, wounds, and diarrhea in Southeast Asia—that is, the fruit hull exhibits an anti-inflammatory action—we pharmacologically studied the anti-inflammatory components of the fruit hull of mangosteen. In an earlier study, we examined the effect of γ-mangostin, a tetraoxygenated diprenylated xanthone from the fruit hull of this plant (Fig. 1A), on AA cascade in C6 rat glioma cells, which is well known to be a useful model system for the study of PG production in the astrocytes, and demonstrated that this natural product reduces PGE_2 release from C6 glioma cells with an IC_{50} of approximately 5 μM and potently inhibits the activities of both COX-1 and COX-2 enzymes with the IC_{50} values of approximately 0.8 and 2 μM, respectively, in vitro (Nakatani et al., 2002).

Herein, we describe the first evidence that γ-mangostin directly inhibits IKK activity, which specifically phosphorylates IκB, and thereby prevents its degradation and, as a result, induces a decrease in the expression of COX-2 protein and its mRNA by a suppression of NF-κB–dependent transcription. This study also demonstrated that γ-mangostin inhibited rat carrageenan-induced hind paw edema, an in vivo acute model of inflammation.

Materials and Methods

Materials. PGE_2 was a generous gift from Ono Pharmaceuticals (Osaka, Japan). Fetal bovine serum, horse serum, Ham's F-10 medium, Eagle's minimum essential medium, 3-(4,5-dimethylthiazol-2-yl)-2,5-diphenyltetrazolium bromide (MTT), and NS398, a selective inhibitor of COX-2, were purchased from Cell Culture Laboratory (Cleveland, OH), Dainippon Pharmaceutical Co. Ltd. (Osaka, Japan), Invitrogen (Carlsbad, CA), Nissui (Tokyo, Japan), Dojindo (Kumamoto, Japan), and Calbiochem (San Diego, CA), respectively. Anti-COX-1, anti-COX-2, anti-IκB, anti-phospho-IκB, anti-IKKα/β, and anti-actin antibodies and recombinant IκBα fusion protein (1–317), anti-PGE_2 antibody, and protein A Sepharose 4B were obtained from Santa Cruz Biochemicals (Santa Cruz, CA), Chemicon International (Temecula, CA), and Zymed Laboratories (South San Francisco, CA), respectively. Alkaline phosphatase-conjugated affinity-purified anti-goat IgG and horseradish peroxide-conjugated affinity-purified anti-rabbit IgG were from Rockland (Gilbertsville, PA) and Cell Signaling Technology Inc. (Beverly, MA), respectively. Total RNA extraction and reverse-transcription polymerase chain reaction (RT-PCR) kits, EndoFree Plasmid Maxi Kit, and pRG-TK vector and Dual-Luciferase Reporter Assay System were purchased from Toyobo Engineering (Osaka, Japan), QIAGEN K.K. (Tokyo, Japan), and Promega (Madison, WI), respectively. [^{3}H]PGE_2 (200 Ci/mmol) and [γ-^{32}P]ATP (5000 Ci/mmol) were from PerkinElmer Life and Analytical Sciences (Boston, MA) and Amersham Biosciences Inc. (Piscataway, NJ), respectively. Other chemicals and drugs were of reagent grade or of the highest quality.

Extraction and Isolation of γ-Mangostin. γ-Mangostin (Fig. 1A) was obtained from the fruit hull of *G. mangostana* L. as reported previously (Jefferson et al., 1970). In brief, the dried fruit hull (1 kg) was ground and then extracted with ethanol (10 liters) for 1 h. The ethanol extract was partitioned between ethyl acetate and water to afford an ethyl acetate fraction (87.4 g). The ethyl acetate soluble fraction was dissolved in hexane/ethyl acetate (4:1) and subjected on a silica gel column chromatography (Wakogel C-200, 800 g, a diameter of 11 cm; Wako Pure Chemicals, Tokyo, Japan), and the sample was eluted with a step-wise gradient of hexane/ethyl acetate [3:1 (2 liters), 3:2 (1 liter), 1:1 (1 liter), 2:3 (1 liter), and 3:7 (2 liters)]. After collecting 1400 ml of the first eluent, the subsequent eluent was

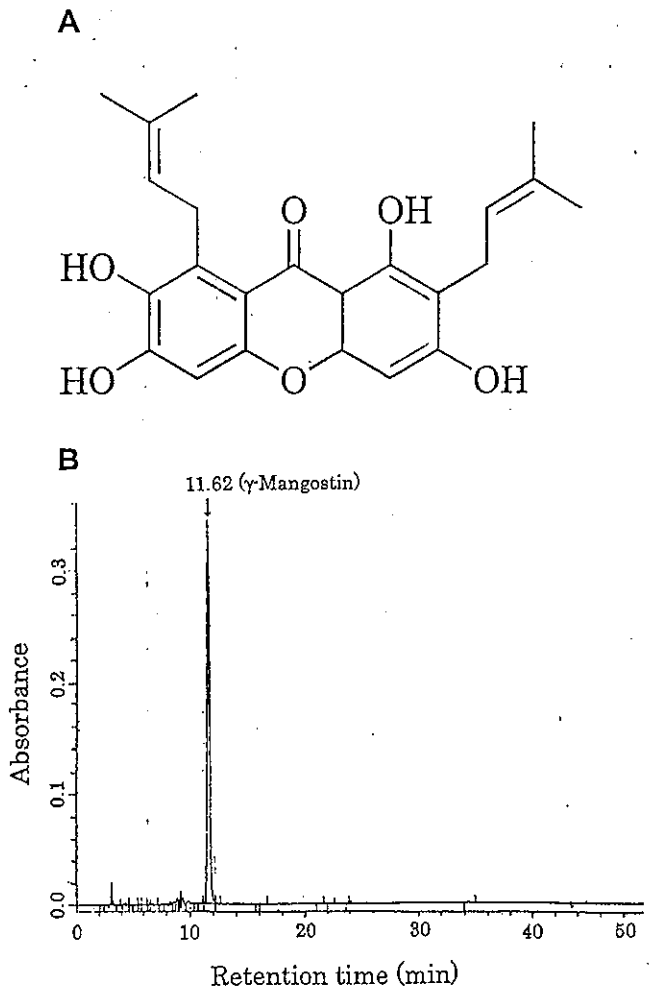

Fig. 1. Chemical structure of γ-mangostin (A) and analysis of purified γ-mangostin by HPLC (B). The elution profile was obtained by monitoring at UV absorbance of 280 nm using an HPLC column (SenshuPak ODS-1251-SS, 4.5 × 250 mm; elution: a linear gradient of 65 to 100% CH_3CN in H_2O at 1 ml/min before which the column was washed with 65% CH_3CN in H_2O for 60 min).

fractionated (200 ml each). Each fraction was monitored by thin layer chromatography [ODS silica gel; acetonitrile/water (8:2) as the developing solvent], and thereby the γ-mangostin-rich fractions, which contained γ-mangostin (R_f = 0.49) but not α-mangostin (R_f = 0.38), were combined. This silica gel column chromatography was performed two times additionally to further obtain the γ-mangostin fraction. The combined γ-mangostin fractions (17.8 g) underwent chromatography on a Senshupak PEGSIL ODS column (20 × 250 mm; Senshu Scientific Co., Tokyo, Japan) and were eluted with methanol/water (4:1 to 1:0) to yield partially purified γ-mangostin (9.0 g). The partially purified γ-mangostin fraction was subjected to an Ultra Pack Silica gel column chromatography (50 mm x 300 mm) (Yamazen, Schaumburg, IL) and eluted with hexane/ethyl acetate (1:1) followed by recrystalization in hexane to finally give purified γ-mangostin (6.0 g). Its purity was more than 90%, as determined by HPLC (SenshuPak ODS-1251-SS, 4.5 × 250 mm; Senshu Scientific) (Fig. 1B). As shown in Fig. 1B, each of the other constituents was less than 3%. Purified γ-mangostin was dissolved in dimethyl sulfoxide (DMSO) to make a concentration of 20 mM as a stock solution and diluted to appropriate concentrations before use.

Cell Culture. C6 rat glioma cells were grown in Ham's F-10 medium containing 15% horse serum and 2.5% fetal bovine serum in a 37°C humidified incubator in an atmosphere of 5% CO_2 in air (Nakatani et al., 2002).

PGE_2 Assay. For PGE_2 assay, C6 cells were seeded onto 12-well plates at a cell density of 1.0×10^5 cells per well. Two days after cell seeding, cells were subjected to the experiment. Cells were cultured for 18 h in culture medium containing vehicle (0.1% DMSO), γ-mangostin, or NS398, a selective inhibitor of COX-2. The conditioned medium was acidified to pH 4.0 by the addition of 1 N HCl, and PGE_2 was extracted twice with ethyl acetate. After ethyl acetate was evaporated under a stream of N_2 gas, the sample was dissolved in 10 mM Tris-HCl, pH 7.6. PGE_2 was determined by radioimmunoassay, as described previously (Nakatani et al., 2002).

Cell Viability Assay. Cell viability for C6 cells was measured using the MTT method as reported previously (Tagliatela et al., 1997). Cells were seeded onto 96-well plates at a cell density of 1.0×10^4 cells per well and cultured with vehicle or γ-mangostin. Twenty-four hours later, cells were subjected to MTT assay. Product formation was monitored by reading the absorbance at 595 nm using a microplate reader (model 450; Bio-Rad, Hercules, CA).

Semi Quantitative RT-PCR. For RT-PCR, C6 cells were seeded onto six-well plates at a cell density of 2.0×10^5 cells per well. Two days later, cells were pretreated with vehicle or γ-mangostin for 1 h and were incubated subsequently with or without 10 μg/ml LPS for 1 h. The total RNA from cells was prepared by using a total RNA extraction kit. Both the COX-1 and COX-2 mRNA levels were semi-quantitatively assayed using an RT-PCR kit as reported previously (Yang et al., 1998) as follows: The sense primers (5′-CTG CTG AGA AGG GAG TTC AT-3′, 602–621 of rat COX-1 cDNA; and 5′-ACA CTC TAT CAC TGG CAT CC-3′, 1229–1248 of rat COX-2 cDNA) and the antisense primers (5′-GTC ACA CAC ACG GTT ATG CT-3′, 981-1000 of rat COX-1 cDNA; and 5′-GAA GGG ACA CCC TTT CAC AT-3′, 11794-1813 of rat COX-2 cDNA) were complementary to the conserved regions of the cDNAs (Yang et al., 1998). The cDNA fragments were amplified 32 cycles (94°C for 60 s, 62°C for 60 s, and 72°C for 60 s). It was demonstrated that this condition for RT-PCR quantitatively yielded PCR product by our preliminary experiments (data not shown). Glyceraldehyde-3-phosphate dehydrogenase mRNA was used as an internal control for the present semiquantitative RT-PCR. PCR products for COX-1 and COX-2 mRNAs were separated by 2% agarose gel electrophoresis, detected by ethidium bromide staining, and subjected to quantitative analysis using an image scanner (Foto/Eclipse; Fotodyne, Hartland, WI). Furthermore, after purification of the PCR products by electrophoresis and filtration, the nucleotide sequences were determined by the dideoxy nucleotide chain termination method to verify that these PCR products are derived from COX-1 and COX-2 mRNAs.

Immunoblotting. For immunoblotting, C6 cells were seeded onto six-well plates at a cell density of 2.0×10^5 cells per well. Two days after seeding, the cells were incubated with vehicle or γ-mangostin for 1 h at 37°C. After cells were incubated with or without 10 μg/ml LPS for an additional 1 h, the medium was aspirated. The cells were lysed by addition of SDS-PAGE sample buffer (187.5 mM Tris-HCl, 6% SDS, 30% glycerol, and 15% 2-mercaptoethanol, pH 6.8). These protein samples were boiled for 5 min, subjected to SDS-PAGE (8–11% gel), and then transferred electrically onto polyvinylidene difluoride membranes (Immobilon-P; Millipore Corporation, Bedford, MA) by the semidry blotting method. The blots were incubated with 2% bovine serum albumin in Tris-buffered saline containing 0.05% Tween 20 at 25°C for 2 h and incubated with goat anti-COX-1 antibody (0.1 μg/ml), goat anti-COX-2 (0.1 μg/ml), rabbit anti-IκB (0.2 μg/ml), rabbit anti-phospho-IκB (0.2 μg/ml), or rabbit anti-actin (0.2 μg/ml) antibody at 25°C for 2 h. The blots were washed several times and incubated with a 1:1000 to 2000 dilution of alkaline phosphatase-conjugated affinity-purified anti-goat IgG or horseradish peroxide-conjugated affinity-purified anti-rabbit IgG in Tris-buffered saline/Tween 20 containing 2% bovine serum albumin at 4°C overnight. Immunoreactive signals were visualized by incubation of the blots with chemiluminescence assay reagents followed by exposing them to Hyperfilm ECL (Amersham Biosciences).

In Vitro IKK Assay. After 10 min of treatment with 10 μg/ml LPS, C6 cells were washed with phosphate-buffered saline, lysed with ice-cold lysis buffer (2 mM EGTA, 150 mM NaCl, 2 mM dithiothreitol, 1 mM *p*-amidinophenyl methanesulfonyl fluoride hydrochloride, 10 μg/ml leupeptin, 10 μg/ml aprotinin, 1 mM Na_3VO_4, and 10 mM Tris-HCl, pH 7.5), and sonicated to prepare cell extract. IKK proteins were prepared by immunoprecipitation as follows: the cell extract was incubated with 6 μg of anti-IKKα/β antibody at 4°C for 4 h, and the immunocomplex was recovered using protein A Sepharose 4B beads. The IKK protein-bound beads were then washed three times with lysis buffer and were aliquoted to five reaction tubes, including 25 μl of the following kinase reaction mixture: 10 mM $MgCl_2 \cdot 6H_2O$, 0.1 mM Na_3VO_4, 2 mM dithiothreitol, 5 mM β-glycerolphosphate, [γ-^{32}P]ATP, and 25 mM Tris-HCl, pH 7.5. After a 10-min incubation with or without tested concentrations of γ-mangostin at 30°C, 1 μg of IκBα was added as a substrate to each reaction tube, and the reaction mixtures were further incubated for 30 min. The reaction was terminated by the addition of SDS-PAGE sample buffer and fractionated by SDS-PAGE. Phosphorylated IκBα (1–317) was visualized as radioluminogram and quantitatively analyzed with the use of Molecular Imager (GS363; Bio-Rad).

Transient Transfection and Dual Luciferase Assay. C6 cells were plated at a cell density of 3.0×10^4 cells per well on a 24-well plate or 1.2×10^4 cells per well on a 48-well plate. Two days later, the cells were transfected using LipofectAMINE 2000 in serum-free medium according to the manufacturer's recommended method. Cells plated onto 24-well plates were subjected to transfection with 0.475 μg/well pNF-κB-Luc, a firefly luciferase reporter construct containing five repeated NF-κB–responsive elements, or dN-Luc; a reporter plasmid that is deficient in the repeated NF-κB–responsive elements in the pNF-κB-Luc (Hirai et al., 1994). Cells plated onto 48-well plates were also subjected to transfection with 0.4 μg/well of phPES2(−327/+59)-Luc, a firefly luciferase reporter construct containing the human COX-2 gene promoter fragment including NF-κB–responsive element (−223/−214) (Inoue et al., 1995). In addition, to normalize transfection efficiency, C6 cells were cotransfected with 0.025 μg of a *Renilla reniformis* luciferase control vector (phRG-TK). After transfection, cells were cultured in the culture medium for 13 or 20 h and then preincubated with vehicle or γ-mangostin for 3 h. Cells were incubated with or without 1 μg/ml LPS for an additional 13 or 18 h, and then the cells were harvested. Determination of both the firefly and *R. reniformis* luciferase activities was performed using a MiniLumat LB 9506 (Berthold Technologies, Bad Wildbad, Germany) with Dual-Luciferase Reporter Assay System (Promega).

Relative luciferase activity represents the ratio of the activity of firefly luciferase to that of *R. reniformis* luciferase.

Animals. 7-week-old male Wistar rats (weighing 150–170 g) were obtained from Charles River Japan (Yokohama, Japan). All experimental procedures were approved by the Laboratory Animal Care and Use Local Committee of Graduate School of Pharmaceutical Sciences, Tohoku University, and were in accordance with the principles and guidelines on animal care of Tohoku University.

Paw Edema. Paw edema was induced on the left hind paw in each rat by a subplantar injection of 75 μl of sterile saline (0.9% NaCl) containing 1% carrageenan. γ-Mangostin at doses ranging from 1 to 30 mg/kg or the vehicle control (DMSO) was given i.p. 30 min before the carrageenan injection. According to the procedure described previously (Planas et al., 1995), the presence of edema was assessed by measuring the volume of the left hind paw before (V_0) and 5 h after carrageenan injection (V_5). The increase in volume in the inflamed paw was obtained by subtracting the volume measured before the carrageenan injection from the observed value at 5 h and expressed as a percentage: % edema = $[(V_5 - V_0)/V_0] \times 100$.

Data Analysis. IC_{50} values were calculated from nonlinear regression analysis of the data. The data are expressed as the means ± S.E.M., and a significant difference ($P < 0.05$) was analyzed by analysis of variance.

Results

Effect of γ-Mangostin on Spontaneous PGE_2 Release from C6 Cells. Glial cells are an important source of PGs in the CNS (Katsuura et al., 1989). In our earlier report, a short-term (10-min) treatment of C6 cells with γ-mangostin has been demonstrated to reduce A23187 (10 μM)-induced PGE_2 release from the cells (Nakatani et al., 2002). From this finding, we hypothesized that if long-term treatment with γ-mangostin might effectively reduce spontaneous PGE_2 release and/or its production, this compound could be used as a potent anti-inflammatory agent for clinical control of PGE level. Therefore, to first test the possibility, C6 cells were treated with γ-mangostin for 18 h to examine the effect of this compound on the spontaneous release of endogenous PGE_2 from C6 cells. It was revealed that γ-mangostin potently reduced the PGE_2 release in a concentration-dependent manner (Fig. 2A) and that NS398, a selective COX-2 inhibitor, markedly reduced the PGE_2 release at 30 μM (Fig. 2B). γ-Mangostin also had no effect on the cell viability in the concentrations ranging from 0.1 to 30 μM, but at 100 μM, it caused an 80% decrease in the cell viability (data not shown), indicating that this appreciable inhibition of the COX-2–dependent spontaneous PGE_2 release from the cells does not result from a reduction in the cell viability caused by γ-mangostin.

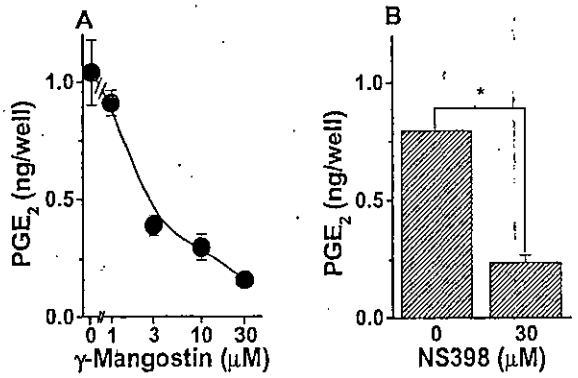

Fig. 2. Concentration-dependent inhibition of endogenous PGE_2 release from C6 cells by γ-mangostin (A) and the effect of NS398 on endogenous PGE_2 release from C6 cells (B). A and B, C6 cells were incubated with the indicated concentrations of γ-mangostin or 30 μM NS398 for 18 h. The released PGE_2 into the culture medium was determined by radioimmunoassay. Each point represents the mean ± S.E.M. ($n = 3$). *, $P < 0.05$ compared with the value for cells treated with 0.1% DMSO (as vehicle control).

Inhibitory Effect of γ-Mangostin on the Expression of Protein and mRNA for COX -2 but Not COX-1 in C6 Cells. COX is a key enzyme for prostaglandin production, because this enzyme is involved in the rate-limiting step in the conversion of AA to prostaglandins (Rosen et al., 1989). Because expression of COX-2 protein and its mRNA are enhanced in response to inflammatory stimuli lasting for several hours (Yamamoto et al., 1995; Inoue and Tanabe, 1998), we next examined whether γ-mangostin affects the expression of COX-1 and COX-2 proteins in C6 cells treated with LPS by immunoblotting. In untreated cells, expressions of COX-1 and COX-2 proteins were detected (Fig. 3, A and B). When treated with LPS, C6 cells showed an increase in protein expression of COX-2 but not COX-1 (Fig. 3, A and B). γ-Mangostin was observed to inhibit this LPS-induced increase in the expression of COX-2 protein in a concentration-dependent manner (Fig. 3B). At 10 μM, this compound also showed a 70% inhibition of the LPS-induced increase in expression of COX-2 protein. In contrast, this compound did not affect the expression of COX-1 protein (Fig. 3A). Furthermore, to examine whether this inhibition of LPS-induced COX-2 protein expression by γ-mangostin results from a reduction in the mRNA level, we analyzed mRNA levels for COX-1 and COX-2 by using RT-PCR. For this assay of mRNA expression of COX-1 and COX-2, an established semiquantitative RT-PCR technique that has been developed recently for determining the regional and temporal profiles of COX-1 and COX-2 mRNA distributions (Yang et al., 1998) was used. Consistent with the results of Western blot analysis described above, γ-mangostin prevented the LPS-induced stimulation of COX-2 mRNA expression in a concentration-dependent manner, with an IC_{50} value of approximately 10 μM in C6 cells, whereas this compound exerted no effect on COX-1 mRNA expression level despite the absence or presence of LPS (Fig. 4, A and B). These results indicate that γ-mangostin may inhibit the expression of COX-2 gene at the transcription level.

Inhibition of NF-κB–Dependent Transcriptional Activation via IKK by γ-Mangostin in C6 Cells. Activation of NF-κB has recently been demonstrated to participate in the induction of expression of COX-2 mRNA by LPS (D'Acquisto et al., 1997) or inflammatory cytokines, including TNF-α (Yamamoto et al., 1995). Therefore, the finding that γ-mangostin prevents the LPS-induced augmentation of expression of COX-2 mRNA in C6 cells raises the possibility that this reduction in expression of COX-2 mRNA by γ-mangostin is the consequence of an inhibition of LPS-induced activation of COX-2 gene transcription through the NF-κB/IκB system. It was thus examined whether γ-mangostin directly influences IKK activity, which phosphorylates IκB protein, using an in vitro IKK assay system. As shown in Fig. 5, γ-mangostin exhibited a concentration-dependent inhibition of the IKK activity with an IC_{50} of approximately 10 μM in vitro, demonstrating that this compound directly inhibits the IKK activity. Next, the phosphorylation and accumulation of IκBα in C6 cells treated with LPS in the absence or presence

of γ-mangostin was analyzed by Western blotting. γ-Mangostin was shown to inhibit the LPS-induced IκB phosphorylation in a concentration-dependent manner and cause an 80% inhibition of the LPS-induced IκB phosphorylation at 10 μM (Fig. 6A). When assayed by Western blotting, it was also shown that γ-mangostin inhibited LPS-induced IκB degradation in a concentration-dependent manner, with an IC_{50} of 10 μM (Fig. 6B). It has been well-documented that proteolytic degradation of IκB is involved in an activation of NF-κB. Thus, to further determine whether treatment with γ-mangostin actually inhibits NF-κB–dependent transcription activity in LPS-induced C6 cells, we conducted transient transfection of C6 cells with pNFκB-Luc, an NF-κB–dependent luciferase reporter plasmid, or dN-Luc, the NF-κB–responsive element-deficient pNFκB-Luc, and assayed the luciferase activity in C6 cells treated with vehicle or γ-mangostin in the absence or presence of LPS. As shown in Fig. 7A, LPS increased the luciferase activity in C6 cells transfected with pNFκB-Luc, whereas LPS-treated cells did not show such an increase in the luciferase activity when transfected with dN-Luc, demonstrating that the LPS-induced stimulation of luciferase activity is NF-κB–dependent. Furthermore, it was shown that at 10 μM, γ-mangostin inhibited the NF-κB–dependent transcriptional activation induced by LPS (Fig. 7A). γ-Mangostin also reduced LPS-induced augmentation of the luciferase activity in C6 cells transfected with phPES2 (−327/+59)-Luc, a human COX-2 reporter gene containing an NF-κB–responsive element, at 30 μM (Fig. 7B).

Inhibition of Rat Carrageenan-Induced Paw Edema by γ-Mangostin. To evaluate the anti-inflammatory activity of γ-mangostin in vivo, rat carrageenan-induced hind paw edema was used as an acute model of inflammation. γ-Mangostin exhibited a concentration-dependent inhibition of the edema and produced remissions of the inflammatory reaction at the doses of 10 and 30 mg/kg, demonstrating that this compound has an anti-inflammatory activity in vivo (Fig. 8).

Discussion

The fruit hull of mangosteen, *G. mangostana*, has been widely used as an anti-inflammatory medicine in Southeast Asia for many years (Mahabusarakam et al., 1987). γ-Mangostin is one of the main constituents contained in the fruit hull of mangosteen. In the present study, we revealed that long-term treatment with γ-mangostin effectively reduced spontaneous PGE_2 release from C6 rat glioma cells, which was shown to be appreciably inhibited by NS398, a selective COX-2 inhibitor, without affecting the cell viability, and that this natural product, like aspirin (Yin et al., 1999), inhibited IKK activity in vitro and consistently reduced LPS-induced NF-κB–dependent transcriptional activation responsible for COX-2 gene transcription, which resulted in the decrease in LPS-induced COX-2 gene expression in C6 cells. Moreover, as expected, γ-mangostin was shown to prevent rat carrageenan-induced hind paw edema used as an acute model of inflammation. We thus suggest that γ-mangostin serves as not only a potent inhibitor of the release of an inflammatory chemical mediator, PGE_2, but also a new inhibitor of COX-2 gene activation and, as a result, acts as an anti-inflammatory agent in vivo.

In this study, we observed that both COX-1 and COX-2 proteins and their mRNA were expressed in the untreated cells. More than 60% of spontaneous PGE_2 release from C6 glioma cells was inhibited by an 18-h treatment with 30 μM NS398, demonstrating that COX-2 mainly contributes to this spontaneous PGE_2 release. In our earlier study, it was demonstrated that suppression of A23187-induced PGE_2 release by γ-mangostin results from its direct inhibition of the COX-1

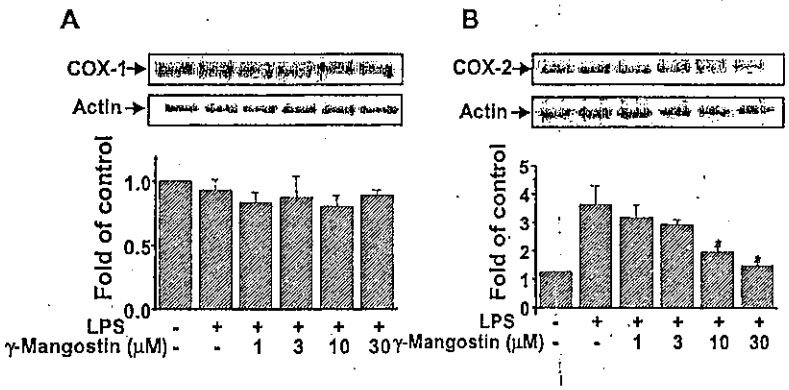

Fig. 3. Decreasing effect of γ-mangostin on the expression of COX-1 (A) and COX -2 (B) proteins as assayed by immunoblotting. After preincubation with the indicated concentrations of γ-mangostin or without this compound for 1 h, cells were incubated in the absence or presence of 10 μg/ml of LPS for 1 h. Shown are representative expression patterns from three independent experiments (top). The densitometric data on the expression of COX-1 and COX -2 proteins (bottom) were calculated as the fold increase of the value for untreated cells. Each column represents the mean ± S.E.M. (n = 3). *, $P < 0.05$ compared with the value for cells treated with 0.1% DMSO (as vehicle control). Actin protein was used as the loading control.

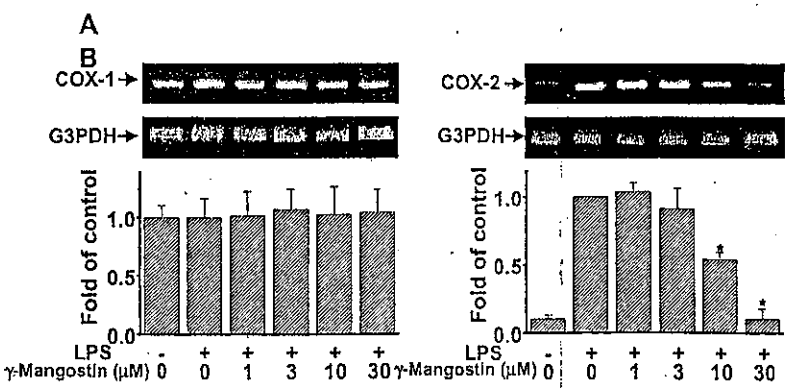

Fig. 4. Decreasing effects of γ-mangostin on COX-1 (A) and COX-2 (B) mRNA expression in C6 cells as measured by RT-PCR. Cells were preincubated with the indicated concentrations of γ-mangostin or without this compound for 1 h and thereafter were incubated in the absence or presence of 10 μg/ml LPS for 1 h. Total RNA from C6 cells was used as a template for cDNA synthesis and then subjected to PCR as described under *Materials and Methods*. Glyceraldehyde-3-phosphate dehydrogenase mRNA was used as the loading control. Shown are representative expression patterns from three independent experiments (top). The densitometric data on COX-1 and COX-2 mRNA expression (bottom) are calculated as the fold increase of the value for cells not treated with γ-mangostin. Each point represents the mean ± S.E.M. (n = 3). *, $P < 0.05$ compared with the value for cells treated with 0.1% DMSO (as vehicle control).

and COX-2 activities in C6 cells, like aspirin and sodium salicylate, nonsteroidal anti-inflammatory drugs (NSAIDs) (Nakatani et al., 2002). COX is the rate-limiting enzyme in the conversion of AA to prostanoids (Rosen et al., 1989). Therefore, we suggest that a marked reduction in the spontaneous PGE_2 release from C6 glioma cells by long-term treatment with γ-mangostin mainly results from a direct inhibition of the COX-2 activity by this natural compound.

Activation of COX-2 gene transcription is mediated by several *cis*-acting promoter elements that respond to multiple intracellular signaling pathways (Mestre et al., 2001); that is, the specific factors involved in the activation of COX-2 gene transcription depend on the cell types and the stimuli. In C6 cells, LPS was observed to stimulate NF-κB– but not activator protein-1–, cAMP-responsive element-, and glucocorticoid response element-dependent transcription (K. Aoki, T. Yamakuni, K. Nakatani, N. Kondo, H. Oku, K. Ishiguro, and Y. Ohizumi, unpublished data). Furthermore, as described above, it was found that LPS induced an increase in the expression of protein and mRNA for COX-2 but not COX-1 in C6 Cells, and that γ-mangostin inhibited the LPS-induced increase in the expression of protein and mRNA for COX-2 in a concentration-dependent manner. The most important finding of the present study is that γ-mangostin has a pharmacological activity of preventing stimulation of NF-κB, a central mediator of inflammation by LPS, by directly inhibiting IKK activity, which resulted in a decrease in LPS-induced phosphorylation and degradation of IκB. This finding raises the possibility that γ-mangostin inhibits IKK activity in vivo to decrease the LPS-induced augmentation of COX-2 gene expression. It was indeed observed that γ-mangostin produced remission of the inflammatory reaction in a concentration-dependent manner, when assayed in an in vivo model of inflammation. It has been shown thus far that aspirin and sodium salicylate inhibit NF-κB activation and IKKβ kinase activity with IC_{50} values of 30 to 50 μM in vitro (Yin et al., 1999) and that these agents suppress LPS-inducible COX-2 gene transcription (Xu et al., 1999). As evaluated using an in vitro assay system, the inhibition of IKK kinase activity by γ-mangostin showed an IC_{50} of approximately 10 μM, although γ-mangostin and these NSAIDs exhibited no chemical structure similarities. On the other hand, antioxidants such as pyrrolidinedithiocarbamate and *N*-acetylcysteine have been reported to inhibit IKK activation in endothelial cells (Spiecker et al., 1998). Taken together, these pharmacological characteristics of this natural product thus provide a plausible explanation for the anti-inflammatory action of the fruit hull of mangosteen, although the precise dual mechanisms of inhibitory actions of γ-mangostin remain to be elucidated.

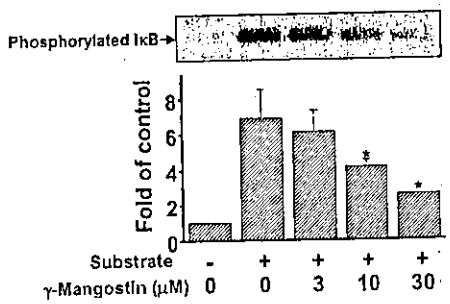

Fig. 5. Concentration-dependent inhibitory effect of γ-mangostin on IKK activity. C6 cells were harvested, lysed, and immunoprecipitated with anti-IKKα/β antibody. The kinase assay was carried out in 25 μl of kinase buffer containing 5 μM ATP, 10 μCi [γ-^{32}P]ATP (5000 Ci/mmol), and 1 μg IκBα (1–317) as a substrate and incubated with the indicated concentrations of γ-mangostin at 25°C for 30 min. The samples were subjected to SDS-PAGE (11% gel). At the top is a representative radioluminogram detected by using a molecular imager (GS363; Bio-Rad). At the bottom, data obtained by densitometry are shown. The results are shown as the fold increase from the value for a sample excluding the substrate and γ-mangostin (0.1% DMSO alone). Each column represents the mean ± S.E.M. (n = 3). *, $P < 0.05$ compared with the value for the sample containing the substrate but not γ-mangostin (as vehicle control).

Astrocytes are a known important, although not the only, source of PGE_2 in the CNS (Katsuura et al., 1989). Their ability to produce PGE_2 upon stimulation with IL-1β, TNF-α, or LPS has been extensively documented (Fontana et al., 1982; Mollace et al., 1998; Molina-Holgado et al., 2000). The increase in PGE_2 levels has been observed in some diseases, including AIDS-associated dementia (Minghetti et al., 1998). Expression of COX-2 in astrocytes has been demonstrated in vitro as well as in vivo. COX-2 expression has been detected in astrocytes of patients suffering from amyotrophic lateral sclerosis (Almer et al., 2001) as well as in astrocytes surrounding the plaques in a mouse model of AD (Matsuoka et al., 2001). Furthermore, the level of astrocytic COX-2 expression in brain tumors was shown to be among the best indicator of tumor progression and severity (Shono et al., 2001). In addition, increased COX-2 expression by tissue macrophages is responsible for the accumulation of large amounts of PGE_2 in local tissues (Smith et al., 2000). Secreted PGE_2 promotes inflammation by increasing vascular permeability and vasodilation and by directing cell migration into the site of inflammation through the induction of inflammatory cytokines (Muraoka et al., 1999). Therefore, the control of PGE_2 production is a critical step in clinically regulating inflammatory reactions during bacterial infection and tissue injury. From the fact that γ-mangostin inhibits stimulation of

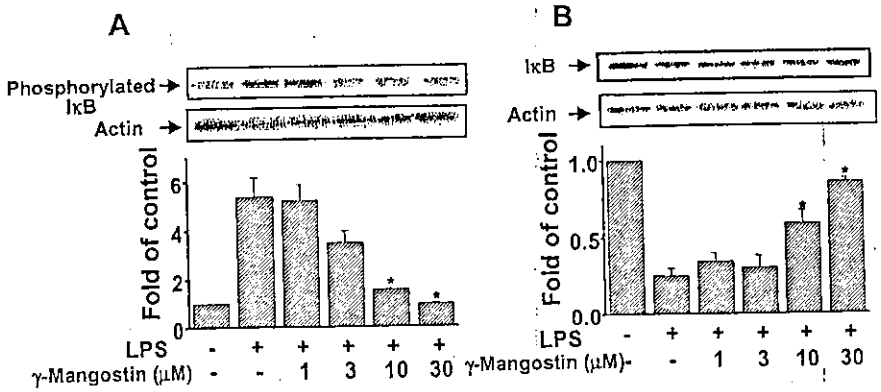

Fig. 6. Concentration-dependent inhibition of LPS-induced phosphorylation (A) and degradation (B) of IκB protein by γ-mangostin in C6 cells. Cells were preincubated with the indicated concentrations of γ-mangostin or without this compound for 1 h and thereafter were incubated in the absence or presence of 10 μg/ml LPS for 0.5 h (A) and 1 h (B). Shown are representative phosphorylation and degradation patterns from three independent experiments (top). The densitometric data on the phosphorylation and degradation of IκB protein (bottom) were calculated as the fold increase of the value for untreated cells. Each column represents the mean ± S.E.M. (n = 3). *, $P < 0.05$ compared with the value for cells treated with 0.1% DMSO (as vehicle). Actin protein was used as the loading control.